UC San Diego
UC San Diego Electronic Theses and Dissertations

Title
Monolayer passivation of semiconductor surfaces

Permalink
https://escholarship.org/uc/item/4281t7dh

Author
Lee, Joon Sung

Publication Date
2011

Peer reviewed|Thesis/dissertation

eScholarship.org Powered by the California Digital Library
University of California

UNIVERSITY OF CALIFORNIA, SAN DIEGO

MONOLAYER PASSIVATION OF SEMICONDUCTOR SURFACES

A dissertation submitted in partial satisfaction of the requirements for the degree

Doctor of Philosophy

in

Materials Science and Engineering

by

Joon Sung Lee

Committee in charge:

Professor Andrew C. Kummel, Chair
Professor Sungho Jin, Co-Chair
Professor Yuhwa Lo
Professor Yuan Taur
Professor Charles W. Tu

2011

Copyright ©

Joon Sung Lee, 2011

All rights reserved.

The dissertation of Joon Sung Lee is approved, and it is acceptable in quality and form for publication on microfilm and electronically:

Co-Chair

Chair

University of California, San Diego

2011

DEDICATION

To Hyeyoung and Jinho

EPIGRAPH

"After all, the future of the world will be decided by you young people. If youth chooses beauty, then there will be more beauty; if it chooses utility, then there will be more useful things. The decision of each individual is of importance not only to oneself but to the whole of mankind."

- From 'Physics and Beyond' by Werner Heisenberg

TABLE OF CONTENTS

SIGNATURE PAGE……………………………………………………………………iii

DEDICATION…………………………………………………………………………..iv

EPIGRAPH………………………………………………………………………………v

TABLE OF CONTENTS………………………………………………………………vi

LIST OF FIGURES……………………………………………………………………..ix

LIST OF ABBREVIATIONS AND SYMBOLS…………………………………xii

ACKNOWLEDGEMENTS……………………………………………………………xv

VITA…………………………………………………………………………………xviii

ABSTRACT OF THE DISSERTATION……………………………………………xx

CHAPTER ONE…………………………………………………………………………1

Introduction

1.1 Passivation of Semiconductor Surface……………………………………………..1

1.2 Dissertation Outline…………………………………………………………………3

1.3 Figures………………………………………………………………………………5

1.4 References…………………………………………………………………………..10

CHAPTER TWO……………………………………………………………………..12

Passivation of Ge(100) Surface via Nitridation

2.1 Abstract……………………………………………………………………………..12

2.2 Introduction…………………………………………………………………………13

2.3 Methods……………………………………………………………………………14

2.4 Results and Discussion……17

2.5 Conclusion……25

2.6 Acknowledgements……26

2.7 Figures……27

2.8 References……36

CHAPTER THREE……39

Passivation of Ge(100) Surface via Oxidation

3.1 Abstract……39

3.2 Introduction……39

3.3 Experimental Details……41

3.4 Results and Discussion……42

3.5 Conclusions……44

3.6 Acknowledgements……44

3.7 Figures……45

3.8 References……49

CHAPTER FOUR……51

Effect of H_2O Chemisorption on Passivation of Ge(100) Surface

4.1 Abstract……51

4.2 Introduction……52

4.3 Experimental Details……54

4.4 Results and Discussion……56

4.5 Conclusions……61

4.6 Acknowledgements……62

4.7 Figures……………………………………………………………………………63

4.8 References…………………………………………………………………………69

CHAPTER FIVE...……………………………………………………………………...72

Nucleation of Trimethylaluminum on Clean and H_2O dosed Ge(100) Surfaces

5.1 Abstract……………………………………………………………………………72

5.2 Introduction………………………………………………………………………73

5.3 Experimental Details……………………………………………………………75

5.4 Results and Discussion…………………………………………………………76

5.5 Conclusions………………………………………………………………………81

5.6 Acknowledgements……………………………………………………………..81

5.7 Figures……………………………………………………………………………83

5.8 References…………………………………………………………………………87

LIST OF FIGURES

CHAPTER ONE

Figure 1.1 STM of aGe(100) surface after ECR nitridation at 500°C…..…………5

Figure 1.2 Bias dependence of STM images of a Ge(100) surface H_2O-dosed at RT…………………………………………………………………6

Figure 1.3 STM of a Ge(100) surface H_2O-dosed at 200°C and at room temperature followed by annealing at 200°C.………………………………………7

Figure 1.4 Filled and empty state STM images of a Ge(100) surface H_2O-dosed at RT followed by annealing at 250°C…….……………………..………………8

Figure 1.5 XPS of a Ge(100) surface after H_2O and TMA dose at RT…………..………9

CHAPTER TWO

Figure 2.1 STM and STS data of a clean Ge(100) surface…………………………27

Figure 2.2 STM of a Ge(100) surface nitrided at room temperature………………..28

Figure 2.3 AES of a Ge(100) surface……………………………………………29

Figure 2.4 STM images and height analysis of a Ge(100) surface nitrided at RT followed by thermal annealing…………………….……………….30

Figure 2.5 STM and STS data of a Ge(100) surface nitrided at 500°C……………31

Figure 2.6 The geometric analysis of the ordered structure of a Ge(100) surface nitrided at 500°C……………………………………………………..32

Figure 2.7 Ball and stick diagram of the ordered Ge subnitride obtained from DFT calculation………………………………………………………………33

Figure 2.8 Ball and stick diagrams of the subnitrided surface and H-passivated subnitride surface……………………………………………………….34

Figure 2.9 Total and Projected Density of States (DOS and PDOS) for the clean Ge, subnitride, and H-passivated systems………………………………..35

CHAPTER THREE

Figure 3.1 STM data of H_2O/Ge(100) before and after post deposition annealing…45

Figure 3.2 STS data of H_2O/Ge(100) before and after post deposition annealing….46

Figure 3.3 STM data of e-beam deposited GeO_2 on Ge(100) before and after post deposition annealing……………………………………………………..47

Figure 3.4 STS data of e-beam deposited GeO_2 on Ge(100) before and after post deposition annealing…………………………………..…………..48

CHAPTER FOUR

Figure 4.1 STM images of clean and H_2O dosed Ge(100) surfaces………………..63

Figure 4.2 STM and STS data of a H_2O dosed Ge(100) surface at RT……………64

Figure 4.3 STM images of annealing experiments of a H_2O-dosed Ge(100) surface…………………………………………………………………..65

Figure 4.4 STM image of a Ge(100) surface H2O-dosed at RT and annealed at 250^oC……………………………………………………………………..66

Figure 4.5 Schematic diagrams of two pathways of H_2 desorption on the H_2O-dosed Ge(100) surface………………………………………………………67

Figure 4.6 STM image of a Ge(100) surface H_2O-dosed at RT and annealed at 300^oC……………………………………………………………………68

CHAPTER FIVE

Figure 5.1 STM and STS data of a TMA dosed Ge(100) surface at RT…………..83

Figure 5.2 STM images and possible structures of a Ge(100) surface dosed with 20,000 L of TMA……………………………………………………………84

Figure 5.3 Relative XPS intensities of surface elements obtained from TMA-only dosed and H_2O+TMA dosed Ge(100) surfaces……………..………….85

Figure 5.4 STM image, line trace analysis, and proposed structure of H_2O pre-dosed Ge(100) followed by TMA dosing at RT and annealing at 200°C……..86

LIST OF ABBREVIATIONS AND SYMBOLS

Å	Ångström (0.1 nm)
Al	aluminum
Ar	argon
AES	Auger electron spectroscopy
ALD	atomic layer deposition
^{o}C	degree Celsius
CB	conduction band
CMOS	complimentary metal oxide semiconductor
C-V	capacitance-voltage
DB	dangling bond
DFT	density functional theory
ΔH_{ads}	enthalpy of adsorption
dI/dV	derivative of the tunneling current with respect to voltage
D_{it}	interfacial density of states
DMA	dimethyl aluminum
DOS	density of states
DV	dimer vacancy
ECR	electron cyclotron resonance
E_F	Fermi level
EOT	equivalent oxide thickness
eV	electron volt

FGA	forming gas annealing
GGA	generalized gradient approximation
Ge	germanium
HPLC	high performance liquid chromatography
III-V	compound semiconductor of groups III and V elements
I_t	tunneling current
K	Kelvin
L	Langmuir (1×10^{-6} Torr seconds)
LDOS	local density of states
ML	monolayer
MMA	monomethyl aluminum
MOSFET	metal oxide semiconductor field effect transistor
N	nitrogen
nA	nanoampere (1×10^{-9} A)
nm	nanometer (1×10^{-9} m)
O	oxygen
PAW	projector augmented wave
PBE	Perdew-Burke-Ernzerhof
RT	room temperature
sccm	standard cubic centimeter per minute
Sb	antimony
Si	silicon
STM	scanning tunneling microscopy

STS	scanning tunneling spectroscopy
TMA	trimethyl aluminum
UHV	ultra high vacuum
VASP	Vienna ab initio simulation package
VB	valence band
V_s	sample voltage

ACKNOWLEDGEMENTS

I would like to acknowledge and thank my advisor, Professor Andrew Kummel, for his support and advice throughout my PhD study. I have learned a lot from his detailed knowledge about surface science and vacuum experiments. I could also learn the efficient and logical way of thinking from the discussion on the challenging problems with him. Especially, I appreciate his support and encouragement to attend all those conferences. It was a great opportunity to improve my presentation and communication skills, develop the ideas of my research, and learn the new topics from the other groups.

I would also like to acknowledge all the committee members, Prof. Sungho Jin, Prof. Yuhwa Lo, Prof. Yuan Taur, and Prof. Charles Tu, for their precious time and reviews of my dissertation.

I would like to thank Prof. Saraswat, Prof. McIntyre, and Prof. Hoyt, for their helpful discussion on the Ge devices from the weekly teleconferences.

I acknowledge Stephen McDonnell and Adam Pirkle from Prof.Wallace group at UT Dallas for their advice on the XPS experiment.

I also acknowledge the Caymax group in IMEC for their collaboration on the TMA/Ge studies.

I must thank the Kummel lab members for being great colleagues and friends of mine during my graduate years. Tyler and Jon showed me how to operate the Park Scientific and Omicron STM systems, Sarah performed all the DFT calculations for the Ge nitridation, Tobin helped the water and TMA experiments with lots of happy hours, Wil helped the STS and XPS experiments, and Sangyeob assisted to install the ion sputter

gun. I also remember all the helps and moments with the other former and present lab members. I believe the time in the Kummel group will remain as a great memory for my life.

I acknowledge Robyn Swanland for her assistance in the travel arrangements and purchase orders, and Charlotte Lauve for her help in all the administrative work involved with MatSci program.

Thanks to Don Johnson and people in the campus research machine shop for their professional assistance in fabricating various parts of the UHV equipments.

Special thanks to the Chungs, the Chois, Donna Kim, Hannah Ka, and Pastor Kim for being great friends of my family in San Diego. I deeply appreciate their friendship and spiritual/nutritional support. Those warm memories with them will be remembered all the time.

I would like to thank my parents and my brother's family (including a baby-to-be-born) in Korea, for their endless support and love. And finally, the most special thanks to Hyeyoung and Jinho, who are the meaning of my life.

The work in this dissertation was funded by the MSD Focus Center Research Program (FCRP-MSD-887.011 and 2051.001).

Chapter 2, in full, is a reprint of the material as it appears in J.S. Lee, S.R. Bishop, T.J. Grassman, and A.C. Kummel, ‘Plasma Nitridation of Ge(100) Surface studied by Scanning Tunneling Microscopy’, *Surf. Sci.* **604,** 1239 (2010). The dissertation author was the primary investigator and author of this paper.

Chapter 3, in full, is a reprint of the material as it appears in J.S. Lee, S.R. Bishop, T. Kaufman-Osborn, E. Chagarov, and A.C. Kummel, ‘Monolayer Passivation of Ge(100) Surface via Nitridation and Oxidation’, *ECS Trans.* **33**, 447 (2010). The dissertation author was the primary investigator and author of this paper.

Chapter 4, in full, has been submitted for publication of the material as it may appear in J.S. Lee, T. Kaufman-Osborn, W. Melitz, S. Lee and A.C. Kummel, 'Effect of H_2O Chemisorption on Passivation of Ge(100) Surface studied by Scanning Tunneling Microscopy', *Surface Science* (2011). The dissertation author was the primary investigator and author of this paper.

Chapter 5, in full, is currently being prepared for submission for publication of the material.as it may appear in J.S. Lee, T. Kaufman-Osborn, W. Melitz, S. Lee and A.C. Kummel, ‘Atomic Imaging of Nucleation of Trimethylaluminum on Clean and H_2O Functionalized Ge(100) Surfaces’, *J. Chem. Phys.* The dissertation author was the primary investigator and author of this material.

VITA

EDUCATION

2011	**Doctor of Philosophy in Materials Science and Engineering** University of California, San Diego
2003	**Master of Science in Physics** Seoul National University, Seoul, Korea
2000	**Bachelor of Science in Physics** Seoul National University, Seoul, Korea

PUBLICATIONS

During the Ph.D

1. **J.S. Lee**, T. Kaufman-Osborn, W. Melitz, S. Lee and A.C. Kummel, 'Atomic Imaging of Nucleation of Trimethylaluminum on Clean and H_2O Functionalized Ge(100) Surfaces', *in preparartion*
2. **J.S. Lee**, T. Kaufman-Osborn, W. Melitz, S. Lee and A.C. Kummel, 'Effect of H_2O Chemisorption on Passivation of Ge(100) Surface studied by Scanning Tunneling Microscopy', *Submitted to Surface Science* (2011)
3. **J.S. Lee**, S.R. Bishop, T. Kaufman-Osborn, E. Chagarov, and A.C. Kummel, 'Monolayer Passivation of Ge(100) Surface via Nitridation and Oxidation', *ECS Trans.* **33**, 447 (2010).
4. **J.S. Lee**, S.R. Bishop, T.J. Grassman, and A.C.Kummel, 'Plasma Nitridation of Ge(100) Surface studied by Scanning Tunneling Microscopy', *Surf. Sci.* **604,** 1239 (2010).
5. W. Melitz, J. Shen, S. Lee, **J.S. Lee**, A.C. Kummel, R. Droopad, and E.T. Yu, 'STS and KPFM Investigation of Fermi Energy Level Pinning Mechanism on InAs and InGaAs Clean Surfaces', *J. Appl. Phys.* **108**, 023711 (2010).
6. J.B. Clemens, S.R. Bishop, **J.S. Lee**, A.C. Kummel, and R. Droopad, 'Initiation of a Passivated Interface between Hafnium Oxide and In(Ga)As(001)-(4×2)', *J. Chem. Phys.* **132**, 244701 (2010).

Prior to the Ph.D

7. Y.S. Kim, I.T. Jeong, J.C. Woo, Z.G. Khim, **J.S. Lee**, H.K. Choi, Y.S. Oh, Kee Hoon Kim, Y.D. Park, and S.H. Chun, 'A Study on the Validity of the Skew Scattering Model for the Anomalous Hall Effect in Low-Temperature Molecular-Beam Epitaxy Gallium Manganese Arsenide', *J. Korean Phys. Soc.* **47**, 306 (2005).

8. **J.S. Lee**, J.D. Lim, K.S. Suh, S.B. Shim, Y.D. Park, C.R. Abernathy, S.J. Pearton, Y.S. Kim, Z.G. Khim, R.G. Wilson, 'AC transport measurement of Mn ion-implanted p^+-GaAs:C', *J. Magn. Magn. Mater*. **272-276**, e1573 (2004).
9. D.P. Norton, M.E. Overberg, S.J. Pearton, K. Pruessner, J.D. Budai, L.A. Boatner, M.F. Chisholm, **J.S. Lee**, Z.G. Khim, Y.D. Park, and R.G. Wilson, 'Ferromagnetism in cobalt-implanted ZnO', *Appl. Phys. Lett*. **83**, 5488 (2003).
10. N.A. Theodoropoulou, A.F. Hebard, D.P. Norton, J.D. Budai, L.A. Boatner, **J.S. Lee**, Z.G. Khim, Y.D. Park, M.E. Overberg, S.J. Pearton, and R.G. Wilson, 'Ferromagnetism in Co- and Mn-doped ZnO', *Solid-State Electronics* **47**, 2231 (2003).
11. **J.S. Lee**, Z.G. Khim, Y.D. Park, D.P. Norton, N.A. Theodoropoulou, A.F. Hebard, J.D. Budai, L.A. Boatner, S.J. Pearton, and R.G. Wilson, 'Magnetic properties of Co- and Mn-implanted $BaTiO_3$, $SrTiO_3$ and $KTaO_3$', *Solid-State Electronics* **47**, 2225 (2003).
12. Y.D. Park, J.D. Lim, K.S. Suh, S.B. Shim, **J.S. Lee**, C.R. Abernathy, S.J. Pearton, Y.S. Kim, Z.G. Khim, and R. G. Wilson, 'Carrier-mediated ferromagnetic ordering in Mn ion-implanted p^+-GaAs:C', *Phys. Rev. B* **68**, 085210 (2003).
13. M.E. Overberg, G.T. Thaler, C.R. Abernathy, N.A. Theodoropoulou, K.T. McCarthy, S.B. Arnason, **J.S. Lee**, J.D. Lim, S.B. Shim, K.S. Suh, Z.G. Khim, Y.D. Park, S.J. Pearton, and A.F. Hebard, 'Growth of the Dilute Magnetic Semiconductor GaMnN by Molecular Beam Epitaxy', *J. Elec. Materials* **32**(5), 298 (2003).
14. **J.S. Lee**, J.D. Lim, Z.G. Khim, Y.D. Park, S.J. Pearton, S.N.G. Chu, 'Magnetic and structural characterization of Co, Cr, V ion-implanted GaN', *J. Appl. Phys.* **93**, 4512 (2003).
15. **J.S. Lee**, Z.G. Khim, Y.D. Park, D.P. Norton, J.D. Budai, L.A. Boatner, S.J. Pearton and R.G. Wilson, 'Effects of Co Implantation in $BaTiO_3$, $SrTiO_3$, and $KTaO_3$', *Electrochem. Solid-State Lett*. **6**, J1 (2003).
16. G.T. Thaler, M.E. Overberg, B. Gila, R. Frazier, C.R. Abernathy, S.J. Pearton, **J.S. Lee**, S.Y. Lee, Y.D. Park, Z.G. Khim, J. Kim and F. Ren, 'Magnetic properties of *n*-GaMnN thin films', *Appl. Phys. Lett*. **80**, 3964 (2002).

FIELD OF STUDY

Major Field: Materials Science Engineering
Studies in Surface Science
Professor Andrew C. Kummel

Major Field: Physics
Studies in Condensed Matter
Professor Zheong-Gu Khim

ABSTRACT OF THE DISSERTATION

MONOLAYER PASSIVATION OF SEMICONDUCTOR SURFACES

by

Joon Sung Lee

Doctor of Philosophy in Materials Science and Engineering

University of California, San Diego, 2011

Professor Andrew C. Kummel, Chair

Professor Sungho Jin, Co-Chair

Germanium is a promising channel material for the next generation MOSFET devices since it has superior electronic properties when compared to silicon. However, high interface trap densities between a Ge surface and a Ge native oxide have been a challenging issue when fabricating practical devices, which demands a proper passivation of the Ge surface. Among various passivation methods, nitridation and oxidation have shown the most promising results. In this study, the monolayer passivation of Ge(100)

surface via formation of Ge-N and Ge-O surface species was investigated using scanning tunneling microscopy (STM) and scanning tunneling spectroscopy (STS).

Direct nitridation was performed on a Ge(100) surface using an electron cyclotron resonance (ECR) plasma source with pure N_2 gas, and a Ge-N ordered structure was formed at 500^oC. However, STS showed that the Fermi level of the n-type Ge(100) surface was pinned near the valence band edge after the nitridation process. Theoretical modeling using DFT calculations showed that the bandgap states are produced from the ordered nitride structure, which is consistent with the Fermi level pinning of the surface. It is predicted that a further passivation process using hydrogen will unpin the Fermi level by reducing the dangling bonds and bond strain of the ordered structure.

Using a differentially-pumped H_2O dosing system, a monolayer of H_2O chemisorption sites on a Ge(100) surface was obtained with a low density of unreacted dangling bonds at room temperature. By annealing up to 250^oC, the coverage of H_2O sites decreased significantly. This is consistent with desorption of H_2 or H_2O, and the multiple prepulsing of H_2O at 250^oC reported by other groups. The H_2O chemisorbed Ge surface is an ideal monolayer passivation of a Ge serving as a great template for the ALD process, since it contains a half monolayer of –OH which induces the formation of Al-O bonds with the introduction of tri-methyl aluminum (TMA). The ability of the H_2O passivated Ge(100) to react with TMA even at 300K was verified with X-ray photoelectron spectroscopy (XPS) experiments which showed thermally unstable Ge-OH bonds have been converted to thermally stable Al-O bonds.

CHAPTER ONE

Introduction

1.1 Passivation of Semiconductor Surface

Atomic structure of semiconductor surfaces has been studied extensively for its importance in the surface science and the semiconductor device technology [1-3]. One of the most critical topics in the semiconductor surface regarding to the technological applications is passivation of semiconductor surfaces. 'Passivation' (or 'surface passivation') is a term used in the semiconductor device process, defined as 'termination of bonds on the semiconductor surface with elements assuring chemical stability of the surface' [4]. A highly-scaled metal-oxide-semiconductor field effect transistor (MOSFET) exploits several atomic layers underneath the gate oxide layer as a carrier channel. Therefore, the electrical property of device such as carrier mobility is severely affected by the quality of interface between the gate dielectric layer and the semiconductor substrate [5-7]. The interface trap density (D_{it}) is a value measured to determine the quality of interface in the MOSFET devices [8]. When the gate oxide layer is deposited on the semiconductor substrate, the unbonded electrons on the surface atom, i.e. dangling bonds, remain on the surface of semiconductor, contributing to increase D_{it}. In the case of a Si-channel MOSFET, these dangling bonds can be 'passivated' by the hydrogen atoms using hydrogen annealing or forming gas annealing (FGA), achieving the D_{it} as low as 10^{10} cm^{-2} [9]. However, in the case of non-Si (e.g. Ge or III-V

compound semiconductors) MOSFET devices, it is very difficult to lower the D_{it} values below 10^{11} cm^{-2}, since the native oxides have poor quality and the hydrogen annealing is ineffective due to the weak bond strength between H and surface atoms.

In the meantime, Ge is a promising channel material for the next generation MOSFET device since it has superior electronic properties (higher electron and hole mobility) compared to Si. However, since the defective interface between Ge/Ge oxide has been one of the challenges in fabricating Ge-channel MOSFET devices, a proper passivation method of a Ge surface is required. While various passivation methods were attempted by many groups [10-16], two different approaches – nitridation [17-19] and oxidation [20-24] - were most extensively studied. Nitridation of Ge is typically performed by the plasma source using pure N_2 or Ar/N_2 mixture [19]. The introduction of nitrogen forms GeO_xN_y or Ge_3N_4 layer on a Ge surface which gives better thermal stability than a Ge native oxide, and suppresses GeO outdiffusion in the post-deposition annealing [25,26]. Stoichiometric GeO_2 generated by ozone or high pressure oxidation is also an effective passivation layer which minimizes the dangling bonds at the interface [22,23]. Another passivation method has been recently reported by Swaminathan et al. as a prepulsing of H_2O on the Ge surface prior to the atomic layer deposition (ALD) of Al_2O_3 [27]. It was found that the surface hydroxylation using H_2O prepulsing significantly reduced the charge trapping, indicating the improvement of interface quality.

For the scaling of equivalent oxide thickness (EOT), however, the thickness of these passivation layers has to be minimized, ideally to one or two monolayers. To achieve a monolayer passivation via nitridation, oxidation, and hydroxylation, it is essential to understand the physical and chemical nature of Ge-N, Ge-O, and Ge-OH

surface species. In this dissertation, the atomic and electronic structures of those surface species were studied and discussed.

1.2 Dissertation Outline

This dissertation mainly focuses the atomic and electronic structures of a Ge(100) surface with nitridation, oxidation, H_2O chemisorption, and trimethylaluminum nucleation to study the monolayer passivation of Ge surface using these methods.

All the experimental data were obtained in the ultrahigh vacuum (UHV) systems at a base pressure below 2×10^{-10} Torr. To clean the native oxides and prepare an atomically flat surface, the Ge(100) sample was sputtered by the Ar^+ ion beam and annealed by direct heating. Surface treatments including nitridation, oxidation, H_2O dosing and TMA dosing were performed *in situ* after the surface cleaning process. To examine the surface structures at an atomistic level, the typical experimental techniques in surface science such as scanning tunneling microscopy (STM), scanning tunneling spectroscopy (STS), Auger electron spectroscopy (AES), and x-ray photoelectron spectroscopy (XPS) were employed.

Chapter 2 presents the study of nitridation of Ge(100) surface at room temperature and at elevated temperature. Electron cyclotron resonance (ECR) plasma was performed to nitride the Ge surface, and the surface species including oxygen displacements, Ge adatoms, and possible Ge-N species were observed at room temperature. Thermal annealing was carried out to differentiate the various adsorbates, and a pure nitride structure remained above 450°C. A highly-ordered Ge nitride structure was formed with

the nitridation at 500°C (Figure 1.1), and the Fermi level (E_F) of n-type Ge sample was found to be pinned near the valence band edge after the nitridaiton. The bonding and electronic structures of the ordered nitride were discussed with the DFT modeling.

Chapter 3 briefly reports the oxidation of Ge(100) surface using GeO_2 and H_2O. The e-beam evaporation of GeO_2 and the H_2O vapor dosing produced different features on the Ge(100) surfaces, and the results were compared with previously studied O_2 dosed Ge(100) surface [28].

Chapter 4 describes the chemisorption of H_2O and its effect on the passivation of a Ge(100) surface. The STM image of the high coverage H_2O chemisorption on Ge(100) was reported for the first time (Figure 1.2). Also, the STS results on the H_2O chemisorption sites and the isolated dangling bond sites were compared. The passivation effect of H_2O chemisorption on Ge(100) was discussed, and the thermal desorption of H_2O at elevated temperature was also investigated (Figures 1.3, 1.4).

Chapter 5 reports the STM and XPS studies of nucleation of TMA on a clean and a H_2O predosed Ge(100) surfaces (Figure 1.5). The STM/STS results of TMA dose on a clean Ge(100) surface at room temperature was presented, followed by thermal behavior of the TMA-induced surface species at elevated temperatures. The effect of H_2O chemisorption on the Al coverage is discussed using XPS data, and finally the monolayer passivation using both H_2O and TMA is suggested.

1.3 Figures

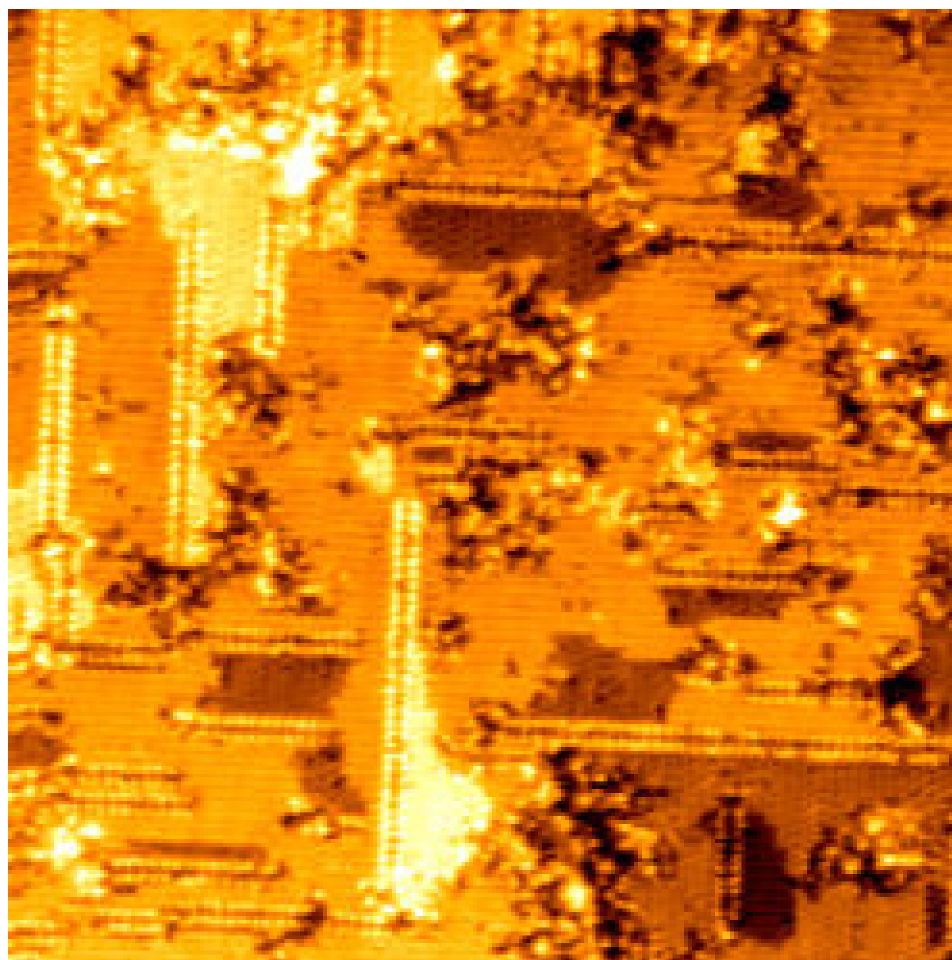

Figure 1.1 STM image (I_t = 0.2 nA, V_s = -2.0 V, 80 nm × 80 nm) of a Ge(100) surface after ECR nitridation at 500°C for 30 minutes followed by annealing at 500°C for 20 minutes.

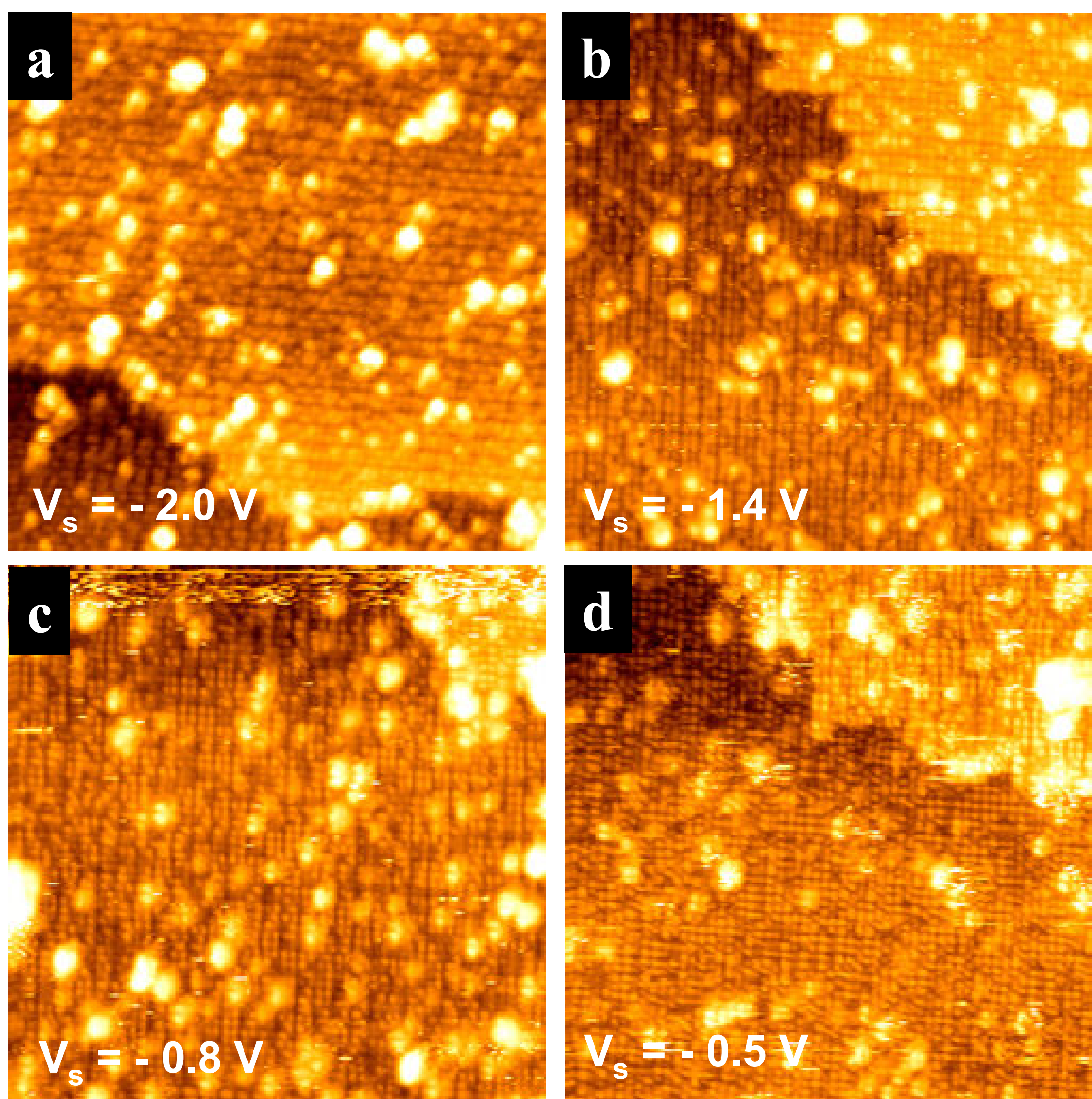

Figure 1.2 STM images (I_t = 0.2 nA, 30 nm × 30 nm) of a Ge(100) surface dosed with 1800 L of H_2O at room temperature. Images are obtained from different regions on the surface. The surface is saturated with H_2O chemisorption sites and the bias dependence of STM image is observed at (a) Vs = -2.0 V, (b) Vs = -1.4 V, (c) Vs = -0.8 V, and (d) Vs = -0.5 V.

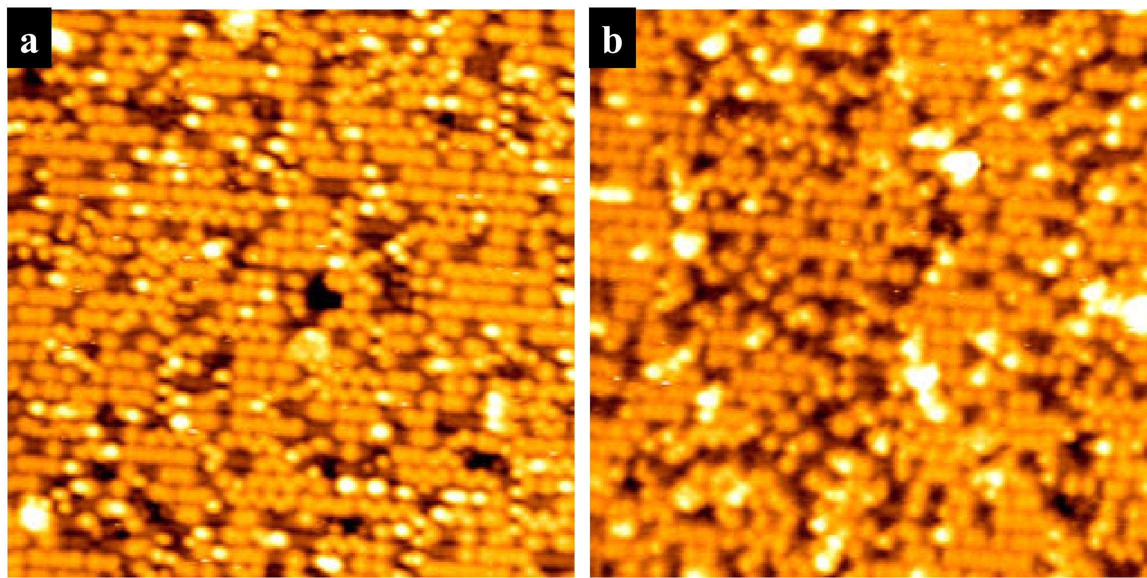

Figure 1.3 STM images (I_t = 0.2 nA, V_s = -2.0 V, 30 nm × 30 nm) of a Ge(100) surface dosed with 1800 L of H_2O (a) at 200°C, and (b) at room temperature followed by annealing at 200°C.

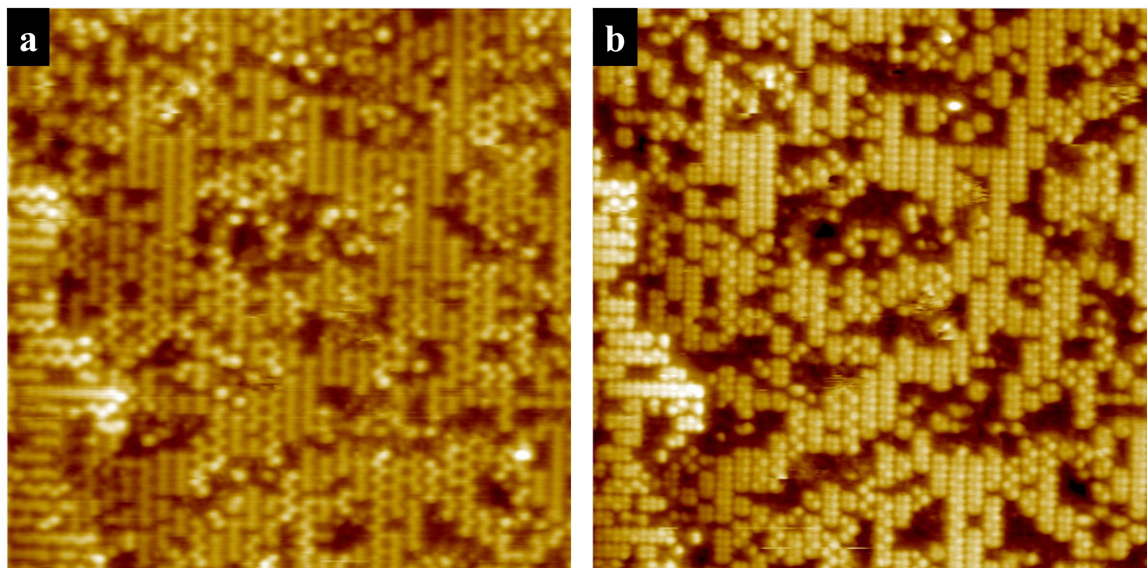

Figure 1.4 Filled state and empty state STM images (I_t = 0.2 nA, 30 nm × 30 nm) of a Ge(100) surface dosed with 1×10^6 L of H_2O at room temperature and annealed at 250°C, measured at (a) V_s = -1.8 V, and (b) V_s = +1.8 V.

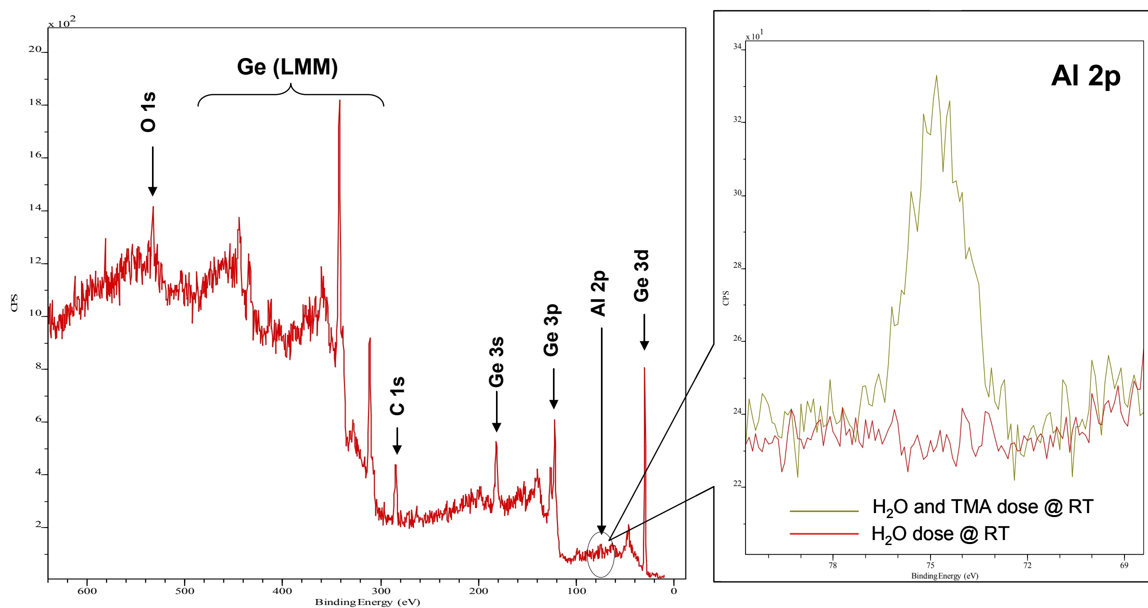

Figure 1.5 XPS of a Ge(100) surface after H_2O and TMA dose at room temperature. The Al *2p* core level before and after the TMA dose is magnified on the right.

1.4 References

[1] C.B. Duke, Chem. Rev. 96 (4) (1996) 1237-1259.

[2] H. Waltenburg, J. Yates_Jr, Chem. Rev. 95 (5) (1995) 1589-1673.

[3] J.A. Kubby, J.J. Boland, Surf. Sci. Rep. 26 (1996) 61-204.

[4] J. Ruzyllo, Semiconductor Glossary: An Introduction to Semiconductor Terminology, Prosto Mutimedia Pub., 2004.

[5] D. Kuzum, T. Krishnamohan, A. Nainani, Y. Sun, P.A. Pianetta, H.-S.P. Wong, K.C. Saraswat, IEEE Trans. Elect. Dev. 58 (1) (2011) 59-66.

[6] T. Maeda, Y. Morita, S. Takagi, Symp. VLSI Tech. Dig. (2010) 213-214.

[7] J. Mitard, et al., Symp. VLSI Tech. Dig. (2009) 82-83.

[8] E.H. Nicollian, J.R. Brews, MOS (Metal Oxide Semiconductor) Physics and Technology, Wiley-Interscience, 1982.

[9] S.M. Sze, Semiconductor Devices - Physics and Technology, John Wiley & Sons, Inc., 2002.

[10] P. Ardalan, E.R. Pickett, J.S. Harris, Jr., A.F. Marshall, S.F. Bent, Appl. Phys. Lett. 92 (25) (2008) 252902.

[11] B. DeJaeger, et al., Microelectron. Eng. 80 (2005) 26.

[12] T. Maeda, S. Takagi, T. Ohnishi, M. Lippmaa, Mat. Sci. Semicon. Proc. 9 (2006) 706.

[13] S. Sun, Y. Sun, Z. Liu, D.-I. Lee, P. Pianetta, Appl. Phys. Lett. 89 (23) (2006) 231925.

[14] N. Taoka, M. Harada, Y. Yamashita, T. Yamamoto, N. Sugiyama, S.-i. Takagi, Appl. Phys. Lett. 92 (11) (2008) 113511.

[15] R. Xie, M. Yu, M.Y. Lai, L. Chan, C. Zhu, Appl. Phys. Lett. 92 (16) (2008) 163505.

[16] R. Xie, C. Zhu, IEEE Elec. Dev. Lett. 28 (2007) 976.

[17] H. Kim, P.C. McIntyre, C.-O. Chui, K.C. Saraswat, M.-H. Cho, Appl. Phys. Lett. 85 (14) (2004) 2902.

[18] T. Maeda, T. Yasuda, M. Nishizawa, N. Miyata, Y. Morita, S. Takagi, J. Appl. Phys. 100 (1) (2006) 014101.

[19] T. Sugawara, R. Sreenivasan, P.C. McIntyre, J. Vac. Sci. Technol. B 24 (5) (2006) 2442.

[20] F. Bellenger, M. Houssa, A. Delabie, V. Afanasiev, T. Conard, M. Caymax, M. Meuris, K. DeMeyer, M.M. Heyns, J. of Electrochem. Soc. 155 (2) (2008) G33-G38.

[21] A. Delabie, F. Bellenger, M. Houssa, T. Conard, S. VanElshocht, M. Caymax, M. Heyns, M. Meuris, Appl. Phys. Lett. 91 (8) (2007) 082904.

[22] D. Kuzum, T. Krishnamohan, A.J. Pethe, A.K. Okyay, Y. Oshima, Y. Sun, J.P. McVittie, P.A. Pianetta, P.C. McIntyre, K.C. Saraswat, IEEE Elec. Dev. Lett. 29 (4) (2008) 328.

[23] C.H. Lee, T. Tabata, T. Nishimura, K. Nagashio, K. Kita, A. Toriumi, ECS Trans. 19 (1) (2009) 165-173.

[24] H. Matsubara, T. Sasada, M. Takenaka, S. Takagi, Appl. Phys. Lett. 93 (3) (2008) 032104.

[25] T. Maeda, M. Nishizawa, Y. Morita, S. Takagi, Appl. Phys. Lett. 90 (7) (2007) 072911.

[26] S.J. Wang, J.W. Chai, J.S. Pan, A.C.H. Huan, Appl. Phys. Lett. 89 (2) (2006) 022105.

[27] S. Swaminathan, Y. Oshima, M.A. Kelly, P.C. McIntyre, Appl. Phys. Lett. 95 (3) (2009) 032907.

[28] T.J. Grassman, S.R. Bishop, A.C. Kummel, Surf. Sci. 602 (14) (2008) 2373-2381.

CHAPTER TWO

Passivation of Ge(100) Surface via Nitridation

2.1 Abstract

The geometric and electronic structures of the surface species on Ge(100) after plasma nitridation were investigated in this study. An electron cyclotron resonance (ECR) plasma source was used to directly nitride Ge(100), and scanning tunneling microscopy and spectroscopy (STM/STS) were employed to study the structures of the nitrided surface. Nitridation at room temperature generated a large diversity of adsorbate sites on the surface containing N, O, and displaced Ge atoms, differentiated by annealing between 200°C and 450°C. Conversely, nitridation at 500°C produced Ge-N adsorbate sites which formed ordered and disordered structures on the surface free from oxygen. Density functional theory (DFT) simulations were performed focusing on the ordered nitride structure, and the simulated surface structure showed a good correspondence with the STM data. DFT calculations also found an increase of density of states near the Fermi level on the ordered nitride structure, which is consistent with the Fermi level pinning observed in the STS results. The DFT results predict H-passivation can unpin the Fermi level of the nitrided surface by reducing the dangling bonds and the bond strain, but the residual plasma damage and the low nitridation rate in UHV are challenges to obtain complementary experimental results.

2.2 Introduction

As the scaling of Si-based metal-oxide-semiconductor field effect transistors (MOSFETs) approaches its physical limits, there have been an increasing number of studies of alternative channel materials. Ge has been considered one of the candidates for the new channel material of the next generation MOSFET devices due to its high electron and hole mobility compared to Si. The success of fabricating silicon transistors has relied on an electrically passive SiO_2/Si interface, even when employing high-k dielectrics [1,2]. However, unlike SiO_2, Ge native oxide (GeO_2) is thermally unstable [3] and water soluble [4] which makes it very challenging to fabricate a GeO_2/Ge-based MOS structure comparable to the SiO_2/Si MOS structure with similar process methods. Moreover, the hydrogen passivation via forming gas annealing (FGA) - usually adopted in the Si MOSFET process - is often ineffective at sufficiently reducing the interface states in the GeO_2/Ge interface [5,6]. Therefore, it is crucial to find a way to electrically passivate the Ge surface which can generate a thermally stable and high density layer on Ge to initiate the Ge-based MOS structure.

Several methods have been reported for Ge surface passivation, including epitaxial Si deposition [7,8], halogen (-F, -Cl, -Br) incorporation [9-11], sulfur-passivation [12,13], oxidation to form GeO_2 [14-18], and thermal or plasma nitridation [19-21]. While the best electrical properties are usually obtained on GeO_2 passivated surfaces [14-17], the nitridation of Ge surface, which forms Ge oxynitride (GeO_xN_y) or Ge nitride (Ge_3N_4), showed both enhanced electrical properties compared to unpassivated

Ge and improved thermal stability compared to GeO_2 passivated Ge [22,23]. When Ge oxynitride and Ge nitride are used as an interfacial layer between a Ge substrate and a high-k dielectric film, an effective suppression of Ge (or GeO) out-diffusion from the substrate into the high-k dielectric was observed [21].

Although the passivation of Ge surface using Ge nitride or Ge oxynitride has been well investigated from the device point of view [19,22], there are very few studies about the atomic and electronic structures of the Ge-N surface species, which are essential to understanding the atomic basis of the combined electrical passivation and enhanced thermal stability. In the current study, electron cyclotron resonance (ECR) plasma nitridation and the scanning tunneling microscopy/spectroscopy (STM/STS) were performed on Ge(100) to determine the initial geometric and electronic structures of the Ge nitride-Ge(100) interface. STM provides a unique opportunity to determine the geometry of Ge-N or Ge-O adsorbates with atomic resolution, while STS provides the electronic structure of the interface prior to any perturbation by gate oxide deposition. Theoretical studies were also performed using density functional theory (DFT) to support experimental results.

2.3 Methods

A. Experimental details

All the sample processes and measurements were carried out in an ultrahigh vacuum (UHV) chamber at a base pressure of 2×10^{-10} Torr. A commercially available *n*-type Ge(100) wafer (Sb-doped, 0.005-0.020 Ohm-cm) was cut into a small piece and

transferred immediately into the UHV chamber. To remove Ge native oxides, the sample was sputtered by a 0.9 kV of Ar^+ ion beam (EX05, VG Microtech) at 500°C for 30 min and annealed at 800°C for 20 min. Both Ar^+ ion sputtering and thermal annealing procedures were repeated several times to obtain atomically flat Ge surfaces.

The nitridation of the Ge surface was performed using an ECR plasma source ("Osprey" Plasma Source, Oxford Scientific) operated at 2.45 GHz with pure N_2 gas. During the nitridation process, the plasma source was differentially pumped by a turbomolecular pump. The N_2 gas was provided through a leak valve with a flow rate of 0.6 sccm (standard cubic centimeter per minute). The nitrogen plasma was directed to the sample surface at normal incidence via an aperture between the differentially-pumped plasma source and the main UHV chamber. The pressure in the differentially-pumped source was 5×10^{-5} Torr while the pressure in the UHV chamber was 8×10^{-8} Torr during the ECR operation.

The topography of the sample surface was characterized by STM (Autoprobe VP1, Park Scientific Instrument) with the constant current mode. Filled state STM images were obtained at a sample bias of -2.0 V and a tunneling current of 0.2 nA. STS experiments were performed with the variable-z method using a modulation bias of 0.1 V at 1.4 kHz from an external lock-in amplifier (SR850, Stanford Research Systems).

All sample preparation processes (cleaning, nitridation, and annealing) were performed *in situ* while the Ge sample was mounted on a water-cooled manipulator equipped with direct sample heating electrodes. After each process, the sample was transferred to the STM for imaging the surface. Auger electron spectroscopy (AES) was performed after the STM/STS measurements to analyze the surface species.

B. Computational methods

Density functional theory (DFT) plane wave calculations with periodic boundary conditions were performed using the Vienna Ab-Initio Simulation Package (VASP) [24-27]. All simulations were performed with the Perdew-Burke-Ernzerhof (PBE) variant of the generalized gradient approximation (GGA), and the atoms were modeled using the projector augmented wave (PAW) pseudopotentials that were supplied with VASP [28,29]. A $4 \times 4 \times 1$ Monkhorst-Pack k-point mesh generation scheme led to a total of 4 irreducible k-points in the first Brillouin zone. A plane-wave basis cut-off was set to 450 eV. The structural relaxation of the slab was obtained once the interatomic forces were below 0.01 eV/Å per atom.

The system studied consisted of an Ge(100) slab supercell with a 4×2 surface dimer reconstruction. The Ge slab was 8 atomic layers thick with 12 atomic layers of vacuum. The bottom 3 layers were frozen and H-terminated to simulate bulk-like conditions. Both a single unit cell and a double unit cell in the y-direction were relaxed consisting of 64 and 128 atoms respectively. Low coverage nitrogen sites were simulated on the single unit cell, while the subsurface nitride was simulated on the double unit cell. Energy calculations were determined with respect to both atomic and molecular nitrogen resulting in exothermic and endothermic results respectively. In addition to the atomic structure and corresponding adsorption energies, the electronic structure and simulated STM images were calculated. Within standard DFT, the band gap is underestimated for semiconductor materials. For Ge(100), the simulated electronic structure results do not contain a true bandgap, rather a local minima in the Fermi level region. Conclusions

were made based on whether there is an increase, decrease, or no change of density in the Fermi level region as to whether the N adsorption site impacted the electronic structure of the surface, similarly to previous work [30]. While hybrid exchange functional methods produce accurate electronic structure results [31,32], they are computationally expensive and have not been performed for this study. Grassman et al. found DFT-based STM simulations using the Tersoff-Hamann approach to correspond with experimental STM images of both the clean and oxidized Ge(100)-(4 × 2) surface [33]. Similar DFT methods were employed in this study to correlate experimental results with computational results.

2.4 Results and Discussion

A clean, ordered Ge(100) surface was obtained after several cycles of Ar^+ ion sputtering and thermal annealing. Figure 2.1 (a) shows the filled state STM image obtained from a clean Ge(100) surface with atomically flat and large terraces. On the clean Ge(100), the surface structure with the mixture of (4 × 2) and (2 × 1)-like reconstructions was always observed. It is well known that the (2 × 1)-like reconstruction is a dynamic superposition of buckled dimers of the (4 × 2) reconstruction [34,35]; therefore, the Ge dimers appear flat unless they are frozen by surface defects, adsorbates, or step-edges. In these reconstructions, the surface Ge atoms have half-filled dangling bonds. The dI/dV spectra obtained by STS measurements on the *n*-type surface is presented in Figure 2.1 (b). The conduction band and valence band edges are well

defined in the STS spectra, with the Ge bandgap consistent with reported values (0.67 eV) and the Fermi level located closer to the conduction band edge than the valance band edge as expected for an *n*-type sample. This confirms the Fermi level is unpinned on the clean *n*-type Ge(100) surface. It has been reported that oxidation and impurities tend to pin the Fermi level of Ge(100) near the valance band [33]. For *p*-type Ge(100) samples, the Fermi level is at the valance band edge, making pinned and unpinned *p*-type Ge(100) indistinguishable in STS. Conversely, *n*-type Ge(100) has a Fermi level which shifts from being closer the conduction band to being closer to the valance band when the surface becomes pinned, which is readily observed in STS [33]. Therefore, experiments in this study were performed only on *n*-type Ge(100) to determine the impact of plasma nitridation on the electronic structure of the nitrided Ge(100) interface.

After ECR plasma nitridation of the clean Ge(100) surface at 300 K for 2 minutes, STM images show various adsorbate sites (Figure 2.2). Previously, Grassman et al. studied oxidation of the Ge surface using STM, and identified the O displacement and the Ge ad-atom sites on the oxygen dosed Ge surface [33]. The O displacement site has one or two oxygen atoms replacing a surface Ge atom or dimer; these oxygen sites appear dark in the filled state STM image (0.6 Å or 1.0 Å below the surface), while the displaced Ge ad-atoms bond on top of undisturbed surface Ge dimers and appear bright (1.2 – 1.4 Å above the surface) [33]. The as-nitrided Ge surface has very similar surface features such as dark oxygen-like sites (Figure 2.2, circle), and bright Ge ad-atom sites (Figure 2.2, square). Even though high-purity N_2 gas is employed for the plasma source, trace water or oxygen also can be introduced into the plasma source from the gas line which reacts on the Ge surface during the plasma nitridation [20]. The existence of oxygen

contamination is verified by the Auger spectra obtained from the surface nitrided at 300 K for 30 min which shows the O peak in addition to N and Ge (Figure 2.3). Meanwhile, another kind of bright site (Figure 2.2, hexagon), distinct from Ge ad-species, is also found which has a typical height of 0.8Å above the surface, and is provisionally assigned as nitrogen-related adsorbates.

To verify the assignment of the nitrogen-related site, the 300 K nitrided Ge surface was annealed to elevated temperatures. Since GeO desorbs from Ge surface above 425°C [3] while Ge nitride evaporates above 600°C [23,36], it is expected that the nitrogen-related sites would stay stable on the Ge surface at the annealing temperatures between 425 - 600°C.

Figure 2.4 presents the STM images of the nitrided Ge surface, with corresponding height analysis histograms and annealing conditions. Note that the x-axis in the histogram indicates the height relative to the substrate Ge atoms. Therefore, the peak of total height distribution (blue curve) is defined as 0 Å, corresponding to the height of the background Ge(100) surface. The as-nitrided Ge surface contained bright and dark sites, covering approximately 17 % and 7 % of the surface, respectively (Figure 2.4 (a)). Up to 200°C, no significant changes are observed for the coverage of bright and dark sites (16 % and 6 %), though these sites are partially coalesced into larger bright and dark islands (Figure 2.4 (b)). For the Ge surface annealed at 400°C, the bright sites are reduced to 5% while the dark sites decrease to 0.5 % (Figure 2.4 (c)). Finally, annealing at 450°C results in nearly complete removal of the dark sites, whereas bright sites are still observed covering 2 % of the surface (Figure 2.4 (d)). The disappearance of the dark sites at 450°C is consistent with the O displacement sites observed on the oxygen-dosed

Ge surface [33]. Therefore, the dark sites on the as-nitrided Ge surface are assigned as O displacement sites.

The height distribution of bright sites consists of two components; (i) the distribution centered at 1.2 Å (bright site A), and (ii) the distribution centered at 0.8 Å (bright site B), which are also distinguished by their different behaviors in the annealing process. The fitting curves of components A and B are overlaid on the height distribution of bright sites in Figure 2.4. Bright site A is continuously reduced as the annealing temperature increases (200-400°C), and nearly disappears at 450°C. This is consistent with the thermal behavior of Ge ad-atoms since they diffuse out to step edges at elevated temperatures. On the contrary, bright site B still remains at 450°C, which is not associated with the Ge ad-species because virtually all Ge ad-atoms diffuse out at this temperature [33]. The partial reduction of bright site B is likely due to desorption of metastable oxygen sites which are 0.6-0.9 Å above the surface [33]. Considering thermal behaviors and height differences, bright site A is assigned as Ge ad-atoms and bright site B remaining at 450°C is assigned as N-related adsorbates.

To further investigate purely N-related sites on Ge(100), the plasma nitridation was performed with the substrate temperature at 500°C, which is consistent with a published method of forming a pure nitrided surface [37]. Even though there are several reports on forming a pure Ge nitride layer at lower temperatures [21,36], the annealing study described above implies nitridation at 500°C would eliminate any chance for oxygen to adsorb on the Ge surface during the nitridation. Furthermore, the nitridation time was increased to 30 minutes to produce a higher coverage of the Ge nitride. Figure 2.5 (a) shows the STM image of the Ge(100) after nitridation at 500°C for 30 min

followed by UHV annealing at 500°C for an additional 5 min. During annealing, the pressure in the UHV chamber was maintained at 2×10^{-10} Torr. Highly ordered structures along the surface Ge dimer rows (Figure 2.5 (a), rectangle) are observed with disordered features (Figure 2.5 (a), oval) and dark sites (Figure 2.5 (a), diamond). Within the detection limit of AES, Auger spectra showed that the Ge(100) surface nitrided at 500°C contains only N while the Ge surface nitrided at 300 K contains both N and O (Figure 2.3). Therefore, the ordered features in Figure 2.5 (a) are assigned as Ge-N related surface structures, and the dark sites are assigned as defect sites due to the residual plasma damage rather than O displacements. The disordered features are consistent with Ge or Ge-N clusters, but a definitive assignment is not possible without an extensive DFT modeling. The STS result shows that the Fermi level of the *n*-type surface is pinned near the valence band (Figure 2.5 (b)). The possible causes of Fermi level pinning include the surface states induced from ordered and disordered structures, and the defect sites due to plasma damage. The Fermi level pinning of the Ge surface with plasma nitridation could be confirmed by photoelectron spectroscopy (PES) which was not performed in this study due to lack of equipment, nor was available in the literature at the time of submitting this manuscript.

In Figure 2.6, the geometry of the ordered structure is analyzed using line traces on the STM image of the 500°C annealed nitrided surface. The ordered structures always appear as paired rows of bright spots parallel to the (4×2)-reconstructed Ge dimer rows neighboring them. The spacing between each row is 11 Å +/- 0.5 Å (line trace a), apparently wider than the distance between two dimer rows of Ge(100)-(2×1) reconstruction (8 Å) (line trace c). The height of the rows relative to the Ge surface is 0.6

to 0.8 Å (line trace a) which is distinct from the typical height of the Ge ad-atom (1.2 to 1.4 Å). The spacing between the neighboring bright spots is 8 Å +/- 0.5 Å (line trace b), which is twice of the spacing between the adjacent Ge dimer rows in the (2 × 1) reconstruction (4 Å) (line trace d). The schematic ball-and-stick diagrams of a Ge-N ordered structure and a Ge(100) (2 × 1) reconstruction satisfying these dimensions are shown at the bottom of Figure 2.6. The ordered structures primarily form at step edges; however, they do exist on the terrace of the Ge(100) surface.

Based on this geometric analysis, the ordered structure was modeled via DFT with two subsurface N atoms under each surface Ge dimer – defined as 'subnitride' in this article. Figure 2.7 shows the atomic structure of the ordered Ge subnitride resulted from the DFT calculation. In this structure, each N atom forms the preferred sp^2-like hybridization with adjacent Ge atoms. The Ge dimer which has two N atoms underneath will be pushed up having slightly higher configuration than the Ge dimers on the surface. The adsorption energy is exothermic with respect to an atomic nitrogen ($\Delta H = -3.77$ eV/N), consistent with the spontaneous formation of the ordered structure in an atomic N ambient and the thermal stability of the structure during high temperature processes (nitridation and anneal at 500°C). However, the adsorbate adsorption is unstable with respect to molecular N_2 ($\Delta H = 1.45$ eV/N); consistent with the observation of low coverage, even with long exposures of atomic nitrogen. After full relaxation, the Ge dimers on the subnitride structure are tilted symmetrically with the outer Ge atoms pointing upward. The distance between these two outer Ge atoms is 11.4 Å, and the height from the surface to one of the outer Ge atom is 0.93 Å. The distance between the Ge dimers with subsurface N atoms along the row direction is 8.0 Å. This is consistent

with the experimental values (11Å, 0.8Å, and 8 Å) obtained by the geometric analysis in Figure 2.6. The STM simulation on this structure correlates well with the experimental STM image as shown in Figure 2.5 (a).

The Ge subnitride structure, shown in Figure 2.7, is capped with dicoordinated Ge atoms which have partially-filled dangling bonds. If left unpassivated, these partially-filled dangling bonds are both highly reactive and very likely to create midgap states which pin the Fermi level. However, in a real passivation layer, an oxide layer would be deposited on top of the Ge nitride which will certainly bind to the Ge dangling bonds [39,40]. The hydrogen passivation of surface atoms acts as a simplified model of oxide bonding and/or a model of post oxide deposition hydrogen passivation of residual dangling bonds. Therefore, the electronic properties of the subnitride structure can be elucidated by performing a DFT calculation of the density of states considering the effect of H-passivation.

For the DFT modeling, H atoms are bonded to all dangling bonds created by subnitride formation to maximize the effect of H-passivation. It was necessary to passivate the di-coordinated Ge dimer atoms directly bonded to the N with two H atoms, and the nearest neighbor tri-coordinated Ge dimer atoms with one H. After H-passivation, the tilt of Ge dimers is completely removed on the subnitride structure (Figure 2.8).

Figure 2.9 (b) depicts the total density of states (DOS) of the clean Ge(100) structure, subnitride structure, and H-passivated structure. Comparing the DOS for unpinned Ge(100) (dotted black curve) with the subnitride structure (blue curve), a large increase of density at the Fermi energy occurred on the subnitride structure suggesting pinning states in the Fermi level region, which is consistent with the observed STS results.

However, the density near the Fermi energy disappears upon H-passivation of the subnitride surface (red curve) with a DOS that resembles the DOS for the clean Ge(100) surface. The DFT results suggest the Fermi level can be unpinned upon H-passivation or even the deposition of an oxide layer which bonds covalently to the under-coordinated Ge atoms with a similar electronic structure to the clean Ge(100) surface.

To further determine the cause of the Fermi level pinning and unpinning, the projected density of states (PDOS), or density of states localized on each atom, of selected atoms (depicted in Figure 2.9 (a)) on the subnitride structure were also calculated. It is found that the Ge atom in the top layer dimer of subnitride (Ge12 in Figure 2.9 (a)) gives the largest contribution to the density of states near the Fermi level (blue curve in Figure 2.9 (c)). It can be inferred that the Ge atom in the top layer dimer is *sp*-hybridized having two half-filled dangling bonds which result in the formation of states near the Fermi level. However, there are also contributions from the second and third layer Ge atoms as well as N atoms to the states in the Fermi level region (see Figure 2.9 (c)). This suggests the subsurface N atoms induce strain to the surface structure resulting in surface state formation which impacts the electronic structure. Since the subsurface N atom (N1 in Figure 2.9 (a)) is bonded to the Ge atom in the second layer (Ge26 in Figure 2.9 (a)), it can consequently distort the bond angles with all next neighboring Ge atoms (Ge26 and Ge45 in Figure 2.9 (a)) and finally affect their electronic structures.

After H-passivation, there is a large reduction in the PDOS contributions (Figure 2.9 (d)) to near Fermi level states from the atoms which induced Fermi level states on the unpassivated surface. H atoms on the surface Ge atoms induce sp^3-hybridization, eliminating states due to the dangling bonds. The sp^3-hybridization also gives symmetric

bond angles to the surface Ge atoms, eventually removing the dimer tilts. The improvement in electronic structure and increase in bulk-like bonding for the H-passivated subnitride structure are consistent with the dangling bonds and the bond strain caused by subsurface N atoms being the main sources of the Fermi level pinning on the subnitride structure.

The effect of the H-passivation on the subnitride structure can partially explain the improvement of electrical property after forming gas annealing on the high-*k*/GeN/Ge MOS devices [22]. It is also likely that the covalent bonding of an oxide layer would improve the electronic structure of the nitrided Ge(100) surface in a manner similar to H-passivation since the oxide bonding would eliminate dangling bonds and restore sp^3-hybridization. However, the electronic effects of defect sites and disordered features regarding the Fermi level pinning were not clarified in this study. Furthermore, the residual plasma defects and disorders, along with a limited nitridation rate in UHV condition, makes it challenging to obtain the experimental results with ordered subnitride structure at a higher coverage. A careful optimization of plasma nitridation or a different method of nitridation (e.g. atomic layer deposition (ALD)) would be required to avoid plasma damage and disordering, thereby determining the impact on the Fermi level pinning and increasing the coverage of the ordered subnitride structure.

2.5 Conclusions

ECR plasma nitridation of the Ge(100) surface was performed to investigate the geometric and electronic structures of the Ge-N bonds using STM and STS. The plasma

nitridation at room-temperature produced surface structures containing O displacement sites, Ge ad-atoms, and probable N-related adsorbates. The post-nitridation annealing experiments differentiated these adsorbate sites, and finally removed most of O displacements and Ge ad-atoms at 450°C. The nitridation at 500°C for 30 min produced an ordered subnitride structure on Ge(100) surface without O displacements and Ge ad-atoms. However, the Fermi level of this surface is pinned due to the increase of dangling bonds and the bond strain. DFT calculations on the atomic and electronic structures of the ordered subnitride show a good correspondence with the experimental STM and STS results. Finally, simulated H-passivation is found to unpin the Fermi level of the subnitride surface structure by eliminating the partially-filled dangling bonds and by reducing the strain from the subsurface N atoms. The thermal stability of nitride passivation and the effect of nitride passivation with forming gas annealing at the interface between Ge and high-*k* dielectric layer can be partially understood based on the findings of this study.

2.6 Acknowledgements

This work was supported by the MSD Focus Center Research Program (FCRP-MSD-887.011).

Chapter 2, in full, is a reprint of the material as it appears in J.S. Lee, S.R. Bishop, T.J. Grassman, and A.C. Kummel, ‘Plasma Nitridation of Ge(100) Surface studied by Scanning Tunneling Microscopy’, *Surf. Sci.* **604,** 1239 (2010). The dissertation author was the primary investigator and author of this paper.

2.7 Figures

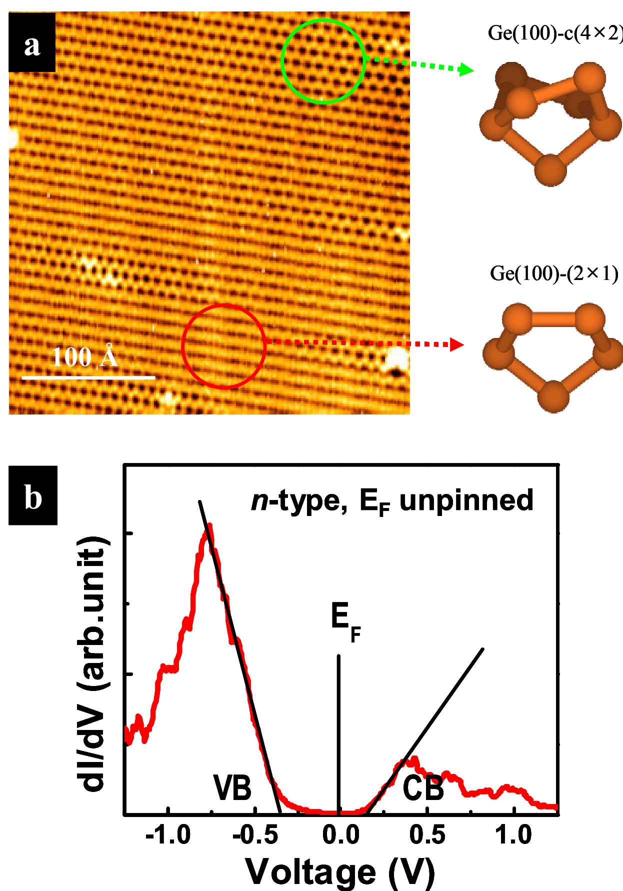

Figure 2.1 (a) (left) Filled state STM image (Vs = -2.0 V, It = 0.2 nA) of a clean Ge(100), and (right) dimer structures of c(4 × 2) (green circle) and (2 × 1) (red circle) surface reconstructions. The Ge dimers normally flip between buckled structures so they appear symmetric (2 × 1) except near defects where they are frozen in the c(4 × 2) structure. (b) STS spectra of clean *n*-type Ge(100). Fermi level (E_F) is located near the conduction band(CB) consistent with an unpinned surface. For Ge(100), pinning states on *n*-type material move the Fermi level to the valance band (VB).

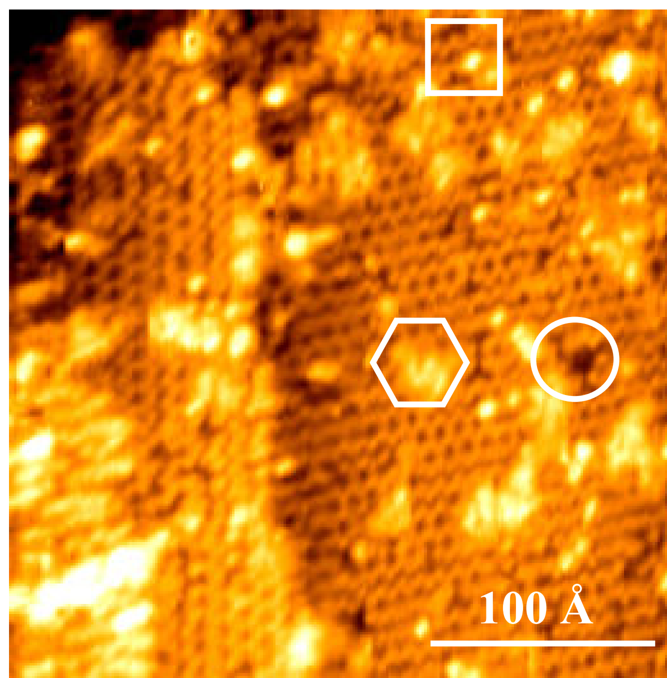

Figure 2.2 Filled state STM image of a Ge(100) surface nitrided at room temperature for 2 min. Dark oxygen-like sites (circle), bright Ge ad-atom sites (square), and bright N-related sites (hexagon) are observed. The Ge ad-atoms and N-related sites can be distinguished by their height and annealing properties.

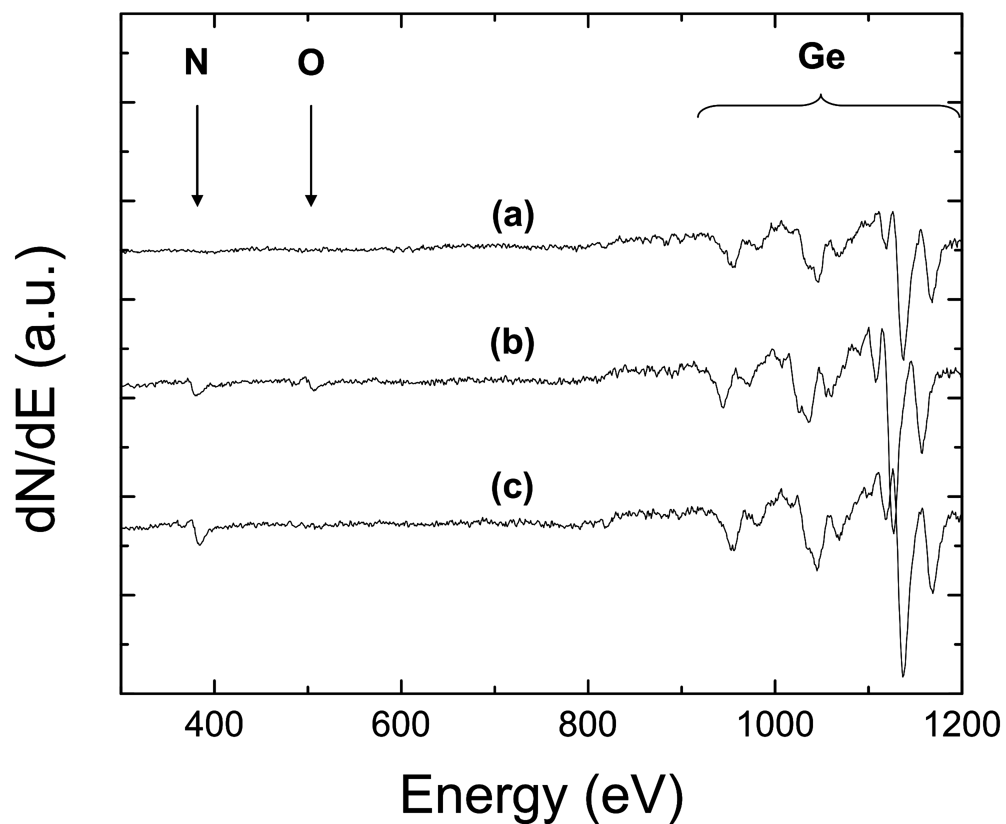

Figure 2.3 Auger electron spectroscopy of Ge(100) surface (a) as-sputtered, (b) after nitridation at room-temperature for 30 min, and (c) after nitridation at 500°C for 30 min. In contrast to the room-temperature nitrided surface, the 500°C nitrided surface is free from oxygen.

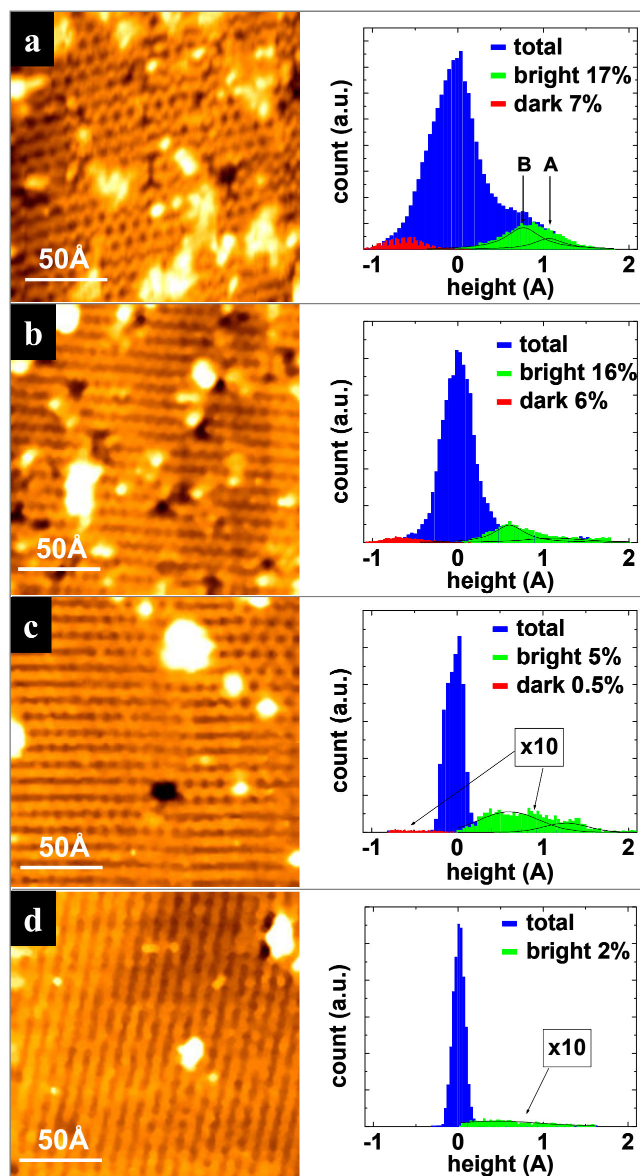

Figure 2.4 STM images and height analysis histograms of Ge(100) surface nitrided at room temperature with (a) no-anneal, (b) 200°C anneal, (c) 400°C anneal, and (d) 450°C anneal. Note that the height is measured relative to the substrate Ge atoms, and the height distributions of bright and dark sites are denoted in green and red colors respectively in the histogram while the total height distribution is represented in blue color. In (c) and (d), bright and dark site distributions are magnified by a factor of 10 for readability purpose. The dark sites are due to O displacements while both Ge ad-atoms (fitting curve A) and N-adsorbates (fitting curve B) contribute to the bright sites.

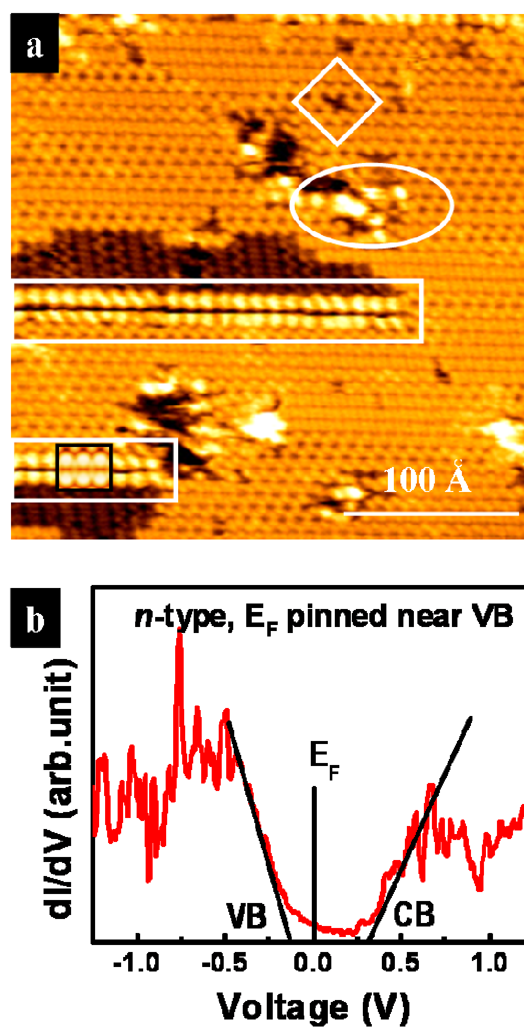

Figure 2.5 (a) Filled state STM image of the *n*-type Ge(100) after nitridation at 500°C for 30 min followed by annealing at 500°C for 5 min. The ordered structures (rectangle), disordered structures (oval), and plasma damage sites (diamond) are observed. The DFT simulated STM image of the ordered structure is overlaid in the black rectangle. (b) STS spectra obtained on the same surface. Fermi level of *n*-type surface is near the valence band (VB) consistent with pinning.

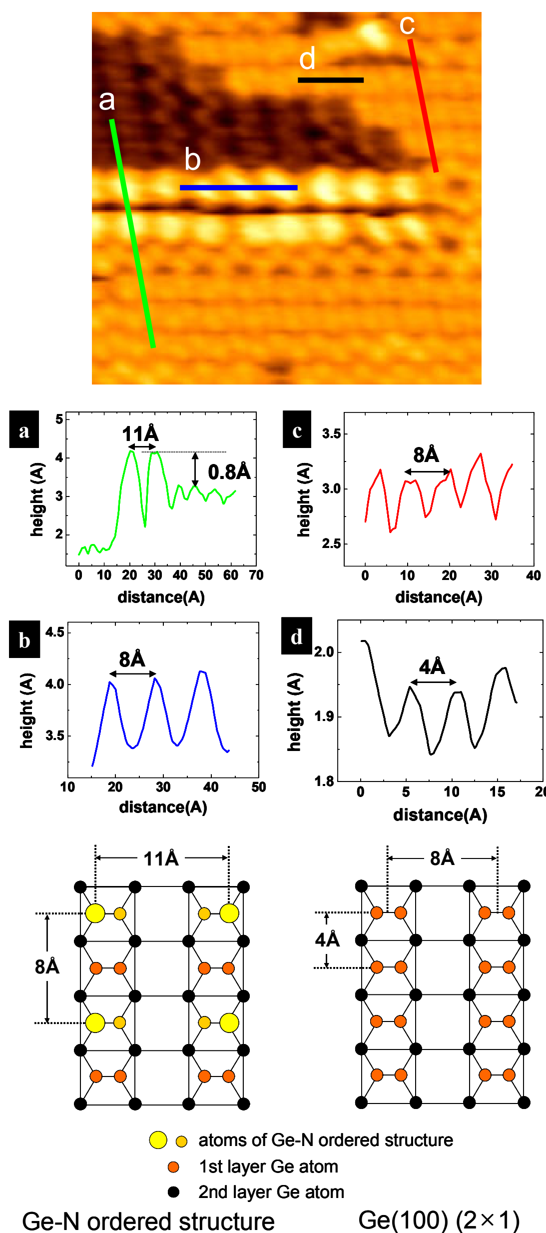

Figure 2.6 The geometric analysis of the ordered structure of 500°C nitrided surface. The rows of ordered structure are 0.8 Å above the (2 × 1) reconstructed surface and separated approximately 11 Å apart along the direction of the line trace a (green), which is wider than the distance between two dimer rows of (2 × 1) reconstruction (8 Å) (line trace c, red). The distance between bright sites along the line trace b (blue) is 8 Å, which is twice of the spacing between dimers in the (2 × 1) reconstruction (line trace d, black). The line traces in the horizontal direction (b and d) are calibrated considering 1.2 times elongation of the STM image due to the thermal drift of the piezoelectric scanner. The schematic ball-and-stick diagrams of the Ge-N ordered structure and (2 × 1)-reconstructed Ge(100) surface are shown at the bottom.

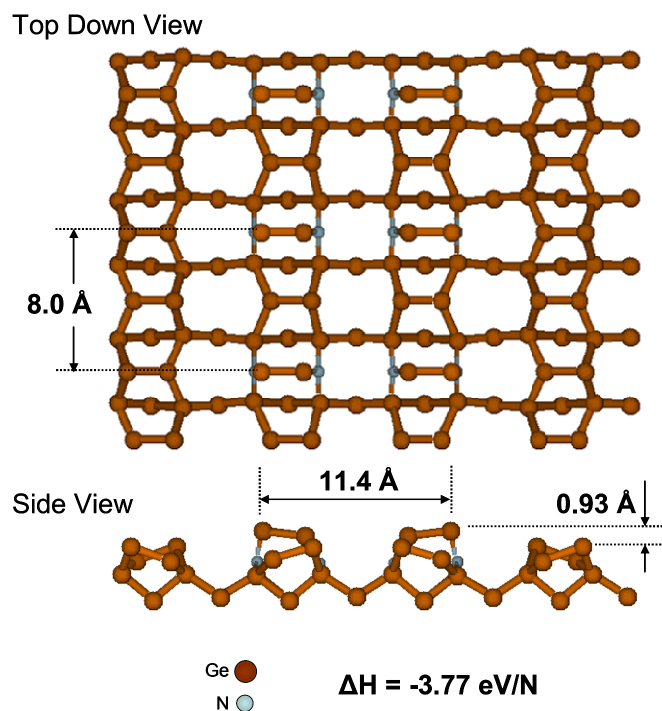

Figure 2.7 Ball and stick diagram of the ordered Ge subnitride obtained from DFT calculation. After full relaxation, the subnitride Ge dimers are tilted symmetrically with the outer Ge atoms pointing upward. The distance between these two outer Ge atoms is 11.4 Å. Also the outer Ge atoms are 0.93 Å above the surface Ge atoms. The subnitride site is exothermic with respect to an atomic nitrogen ($\Delta H = -3.77$ eV/N).

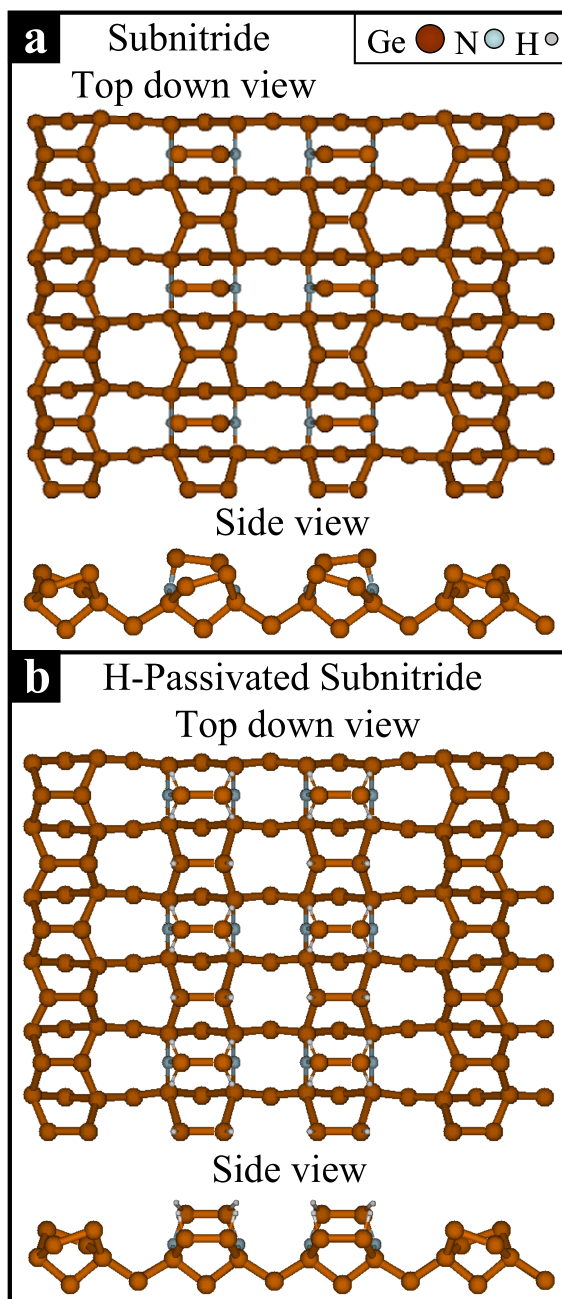

Figure 2.8 Ball and stick diagrams of the (a) subnitride surface and (b) hydrogen passivated subnitride surface with a top down view and side view of the top 3 layers for both systems. H atoms are bonded to all dangling bonds of the Ge atoms on the subnitride structure to maximize the effect of H-passivation. Note the dimer tilt is completely removed by hydrogen passivation.

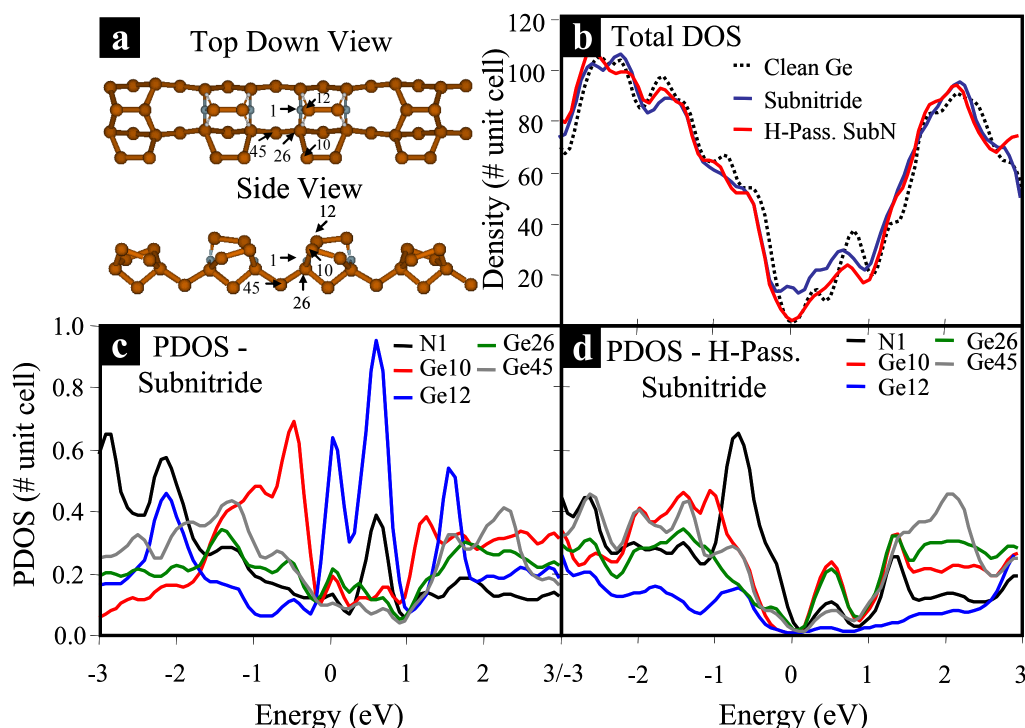

Figure 2.9 Total Density of States (DOS) and Projected Density of States (PDOS) for the clean Ge, subnitride, and hydrogen passivated (H-pass.) systems. (a) Ball and stick diagram with atom # labeled for identification of density contributors in the PDOS. Atom 1 represents N, atom 10 and 12 represent first layer Ge, atom 26 represents second layer Ge and atom 45 represents third layer Ge. (b) Total density of states for the subnitride (blue, with increased density in the Fermi level region) and H-passivated subnitride (red, similar to the clean Ge DOS) compared to the clean Ge substrate (dashed black). (c) Projected DOS for the subnitride surface where all atoms strained by the subnitride contain density in the Fermi level region, with the largest contribution from the first layer dimer atoms. (d) PDOS for the H-passivated subnitride surface which shows the density is reduced for the atoms strained by the subnitride.

2.8 References

[1] G.D. Wilk, R.M. Wallace, J.M. Anthony, J. Appl. Phys. 89 (10) (2001) 5243.

[2] M. Copel, M. Gribelyuk, E. Gusev, Appl. Phys. Lett. 76 (4) (2000) 436.

[3] K. Prabhakaran, F. Maeda, Y. Watanabe, T. Ogino, Thin Solid Films 369 (1-2) (2000) 289-292.

[4] CRC Handbook of Chemistry and Physics, Boca Raton, CRC Press, 1989.

[5] M. Stutzmann, J.-B. Chevrier, C.P. Herrero, A. Breitschwerdt, Appl. Phys. A: Solids Surf. 53 (1) (1991) 47.

[6] V.V. Afanas'ev, Y.G. Fedorenko, A. Stesmans, Appl. Phys. Lett. 87 (3) (2005) 032107.

[7] B. DeJaeger, et al., Microelectron. Eng. 80 (2005) 26.

[8] N. Taoka, M. Harada, Y. Yamashita, T. Yamamoto, N. Sugiyama, S.-i. Takagi, Appl. Phys. Lett. 92 (11) (2008) 113511.

[9] R. Xie, M. Yu, M.Y. Lai, L. Chan, C. Zhu, Appl. Phys. Lett. 92 (16) (2008) 163505.

[10] S. Sun, Y. Sun, Z. Liu, D.-I. Lee, P. Pianetta, Appl. Phys. Lett. 89 (23) (2006) 231925.

[11] P. Ardalan, E.R. Pickett, J.S. Harris, Jr., A.F. Marshall, S.F. Bent, Appl. Phys. Lett. 92 (25) (2008) 252902.

[12] T. Maeda, S. Takagi, T. Ohnishi, M. Lippmaa, Mat. Sci. Semicon. Proc. 9 (2006) 706.

[13] R. Xie, C. Zhu, IEEE Elec. Dev. Lett. 28 (2007) 976.

[14] A. Delabie, F. Bellenger, M. Houssa, T. Conard, S. VanElshocht, M. Caymax, M. Heyns, M. Meuris, Appl. Phys. Lett. 91 (8) (2007) 082904.

[15] F. Bellenger, M. Houssa, A. Delabie, V. Afanasiev, T. Conard, M. Caymax, M. Meuris, K. DeMeyer, M.M. Heyns, J. of Electrochem. Soc. 155 (2) (2008) G33-G38.

[16] D. Kuzum, T. Krishnamohan, A.J. Pethe, A.K. Okyay, Y. Oshima, Y. Sun, J.P. McVittie, P.A. Pianetta, P.C. McIntyre, K.C. Saraswat, IEEE Elec. Dev. Lett. 29 (4) (2008) 328.

[17] H. Matsubara, T. Sasada, M. Takenaka, S. Takagi, Appl. Phys. Lett. 93 (3) (2008) 032104.

[18] C.H. Lee, T. Tabata, T. Nishimura, K. Nagashio, K. Kita, A. Toriumi, ECS Trans. 19 (1) (2009) 165-173.

[19] H. Kim, P.C. McIntyre, C.-O. Chui, K.C. Saraswat, M.-H. Cho, Appl. Phys. Lett. 85 (14) (2004) 2902.

[20] T. Sugawara, R. Sreenivasan, P.C. McIntyre, J. Vac. Sci. Technol. B 24 (5) (2006) 2442.

[21] T. Maeda, T. Yasuda, M. Nishizawa, N. Miyata, Y. Morita, S. Takagi, J. Appl. Phys. 100 (1) (2006) 014101.

[22] T. Maeda, M. Nishizawa, Y. Morita, S. Takagi, Appl. Phys. Lett. 90 (7) (2007) 072911.

[23] S.J. Wang, J.W. Chai, J.S. Pan, A.C.H. Huan, Appl. Phys. Lett. 89 (2) (2006) 022105.

[24] G. Kresse, J. Hafner, Phys. Rev. B 47 (1) (1993) 558.

[25] G. Kresse, J. Furthmüller, Phys. Rev. B 54 (16) (1996) 11169.

[26] G. Kresse, Thesis, Technische Universität Wien, 1993.

[27] G. Kresse, J. Furthmüller, Comp. Mat. Sci. 6 (1) (1996) 15.

[28] P.E. Blöchl, Phys. Rev. B 50 (24) (1994) 17953.

[29] G. Kresse, D. Joubert, Phys. Rev. B 59 (3) (1999) 1758.

[30] T.J. Grassman, S.R. Bishop, A.C. Kummel, Microelectron. Eng. 86 (3) (2009) 249-258.

[31] P. Broqvist, A. Alkauskas, A. Pasquarello, Phys. Rev. B 78 (7) (2008) 075203.

[32] P. Broqvist, J.F. Binder, A. Pasquarello, Appl. Phys. Lett. 94 (14) (2009) 141911.

[33] T.J. Grassman, S.R. Bishop, A.C. Kummel, Surf. Sci. 602 (14) (2008) 2373-2381.

[34] T. Sato, M. Iwatsuki, H. Tochihara, J. Electron Microscopy 48 (1) (1999) 1-7.

[35] H.J.W. Zandvliet, Physics Reports 388 (2003) 1-40.

[36] K. Kutsuki, G. Okamoto, T. Hosoi, T. Shimura, H. Watanabe, Jpn. J. Appl. Phys. 47 (4) (2008) 2415.

[37] Y. Oshima, Y. Sun, D. Kuzum, T. Sugawara, K.C. Saraswat, P. Pianetta, P.C. McIntyre, J. of Electrochem. Soc. 155 (12) (2008) G304-G309.

[38] P.W. Peacock, J. Robertson, Phys. Rev. Lett. 92 (5) (2004) 057601.

[39] K.-Y. Tse, J. Robertson, J. Appl. Phys. 100 (9) (2006) 093713.

CHAPTER THREE

Passivation of Ge(100) Surface via Oxidation

3.1 Abstract

The monolayer passivation of Ge(100) surface via formation of Ge-O surface species was studied using scanning tunneling microscopy (STM) and scanning tunneling spectroscopy (STS). Two different oxidation methods – H_2O vapor dosing and e-beam evaporation of GeO_2 – were used to form the Ge-O bonds on the Ge(100) surface. Oxidation of Ge(100) using H_2O produced an –OH and –H terminated surface with very few Ge ad-atoms, while e-beam evaporation of GeO_2 formed semi-ordered Ge-O structures and Ge ad-species at room temperature. Annealing above 300°C formed suboxide rows on both H_2O and GeO_2 dosed surfaces, and the scanning tunneling spectroscopy (STS) showed that the Fermi level was pinned near the valence band edge on the *n*-type Ge surfaces covered by suboxides.

3.2 Introduction

Germanium is considered a promising channel material for the next generation MOSFET devices due to its favorable electronic properties (e.g. high electron and hole mobilities) compared to Si. However, high defect densities at the interface between Ge and high-k dielectric layers have been a challenging issue in fabricating scaled devices.

Among several different methods to passivate the Ge surface [1-3], nitridation [4-6] and oxidation [7-11] have shown the most promising results.

Nitridation of Ge has been studied using thermal (NH_3) [4] or a plasma nitridation (atomic N) [5,6] sources to form Ge oxynitride (GeO_xN_y) or Ge nitride (Ge_3N_4). These layers have better thermal stability than Ge oxide [12,13]; therefore, they suppress the GeO outdiffusion from Ge surfaces to the high-k dielectric layer during processing at elevated temperatures, resulting in a low interface defect density [5]. A stoichiometric GeO_2 layer produced by ozone [9] or high pressure oxidation [10] is also effective in passivating Ge surfaces by eliminating interface defects due to suboxides and dangling bonds. However, for a practical MOSFET device with a high-k dielectric layer, these passivation layers should be scaled down to one or two monolayers.

In this study, the geometric and electronic properties of a Ge(100) surface at an initial stage of oxidation were studied; the low coverage reactions are crucial to understanding the physical or chemical origin of defect formation that can occur in the ultrathin passivation layer. Submonolayer structures were formed on a Ge(100) surface by oxidation and were probed using scanning tunneling microscopy and spectroscopy (STM/STS). Oxidation of Ge(100) was performed using H_2O and e-beam evaporation of GeO_2, and the results were compared with the O_2 dosed Ge(100) surface [14].

3.3 Experimental Details

A Ge sample was cut from the *n*-type Ge(100) wafer (Sb-doped, 0.005-0.020 Ohm-cm), and immediately transferred into the ultrahigh vacuum (UHV) chamber at a base pressure of 2×10^{-10} Torr. The native oxide of Ge(100) surface was removed using 0.9 kV Ar^+ ion sputtering at 500°C for 30 min, followed by thermal annealing at 800°C for 20 min. Oxidation of the Ge surface was carried out using two different oxidants; H_2O and GeO_2. H_2O (HPLC grade) was carefully degassed and dosed onto a Ge(100) surface through a differentially-pumped dosing system. E-beam evaporation was used for the deposition of GeO_2 (99.999%, metals basis). The atomic and electronic structures of the sample surface were observed using scanning tunneling microscopy and spectroscopy (STM/STS), while Auger electron spectroscopy (AES) was used to analyze the chemical elements on the surface. All the STM images were obtained at a sample bias of -2.0V and a set point tunneling current of 0.2 nA.

3.4 Results and Discussion

A. Oxidation of Ge(100) using H_2O

Figure 3.1 (a) shows the STM image of a Ge(100) surface dosed with 1.5 L of H_2O at room temperature. The Ge surface is covered by approximately 0.1 monolayers (ML) of dark sites, which are due to the –OH and –H termination of Ge dangling bonds and consistent with the dissociative chemisorption of H_2O on a Ge(100) surface [15]. In the case of the O_2-dosed Ge(100) surface, an equal amount of dark (O displacement) and bright (Ge at-atom) sites were produced due to the strong reactivity of each O atom to displace a Ge surface atom [14]. In contrast, H_2O dosing produces very few Ge ad-atoms, which makes H_2O as a promising oxidant for a monolayer passivation of Ge. However, there are also Ge dimer vacancies (DV) observed on the H_2O dosed surface (Figure 3.1 (a), diamond), which are distinguished from the H_2O adsorbate sites by different depths (0.9 Å for H_2O sites, 1.2 Å for DV). These dimer vacancies are possibly due to H_2O etching resulting in the Fermi level pinning of the *n*-type Ge surface after H_2O dosing (Figure 3.2 (a)).

The dark H_2O sites are significantly reduced when the surface is annealed to 300°C (Figure 3.1 (b)). Instead, primarily bright sites are observed with some dark suboxide rows which are typically observed on the O_2-dosed surface at the same temperature [14]. On the Ge(100) surface, H_2 desorption occurs around 300°C [16]. Therefore, it is assumed that the surface structures remaining at 300°C are mostly due to oxygen. The suboxide species at 300°C can cause the Fermi level pinning (Figure 3.2 (b)),

but E_F moves slightly towards midgap, implying there might be other mechanisms involved in the Fermi level pinning at this temperature.

B. Oxidation of Ge(100) using E-beam evaporation of GeO_2

E-beam evaporation of GeO_2 at room temperature formed semi-ordered structures along the substrate Ge dimer rows and Ge ad-atoms on the Ge(100) surface (Figure 3.3 (a)). It is known that GeO_2 decomposes during e-beam evaporation, producing a substoichiometric film [17]. Hence, the semi-ordered structures on the GeO_2 deposited surface are likely Ge suboxides. It is also known that the Ge suboxide films undergo phase separation into Ge and GeO_2 at elevated temperatures on a Si substrate [18]. However, in the presence of excess Ge, GeO_2 transforms into GeO by the following reaction [19].

$$Ge + GeO_2 \rightarrow 2\ GeO \qquad (1)$$

Therefore, there would be only Ge or Ge suboxides remaining when the GeO_2 deposited Ge(100) surface is annealed at 325°C, consistent with the STM observation of Ge regrowth islands and suboxide rows (Figure 3.3 (b)). The STS of GeO_2 deposited Ge(100) surface indicate the Fermi level of the *n*-type sample surface is pinned near the valence band edge on both unannealed and annealed cases, probably due to the suboxide species (Figure 3.4).

3.5 Conclusions

The atomic and electronic structures of Ge(100) surface after oxidation were investigated for the monolayer passivation of a Ge surface via Ge-O surface species. H_2O dosing at room temperature terminated the dangling bonds on a Ge(100) surface with -OH and -H without displacing surface Ge atoms, while GeO_2 deposition produced semi-ordered Ge-O structures with Ge ad-atoms. However, annealing above 300°C formed suboxide rows on both H_2O and GeO_2 dosed surfaces, causing the Fermi level pinning.

3.6 Acknowledgements

This work was supported by the MSD Focus Center Research Program (FCRP-MSD-2051.001).

Chapter 3, in full, is a reprint of the material as it appears in J.S. Lee, S.R. Bishop, T. Kaufman-Osborn, E. Chagarov, and A.C. Kummel, 'Monolayer Passivation of Ge(100) Surface via Nitridation and Oxidation', *ECS Trans.* **33**, 447 (2010). The dissertation author was the primary investigator and author of this paper.

3.7 Figures

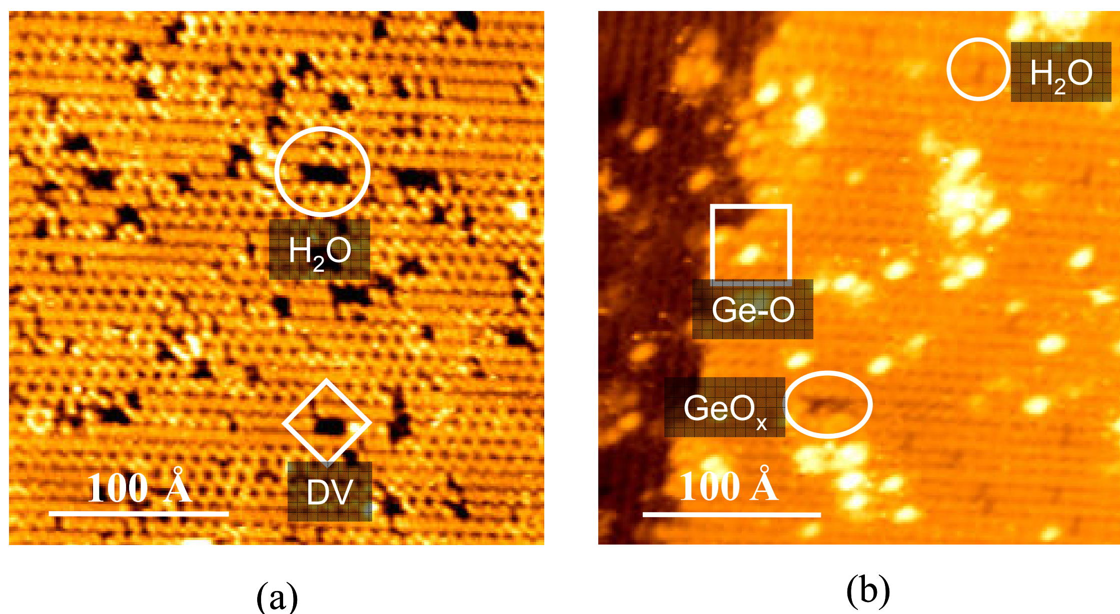

Figure 3.1 STM of H_2O/Ge(100) before and after post deposition annealing. (a) The Ge(100) surface dosed with 1.5 L of H_2O at room temperature. H_2O chemisorption sites (circle) and dimer vacancies (diamond) can be distinguished by different depths (0.9 Å for H_2O sites, 1.2 Å for DV). (b) The H_2O dosed Ge(100) surface after annealing at 300°C. Due to the H_2 desorption at this temperature, H_2O sites (circle) are significantly reduced and bright Ge-O sites (square) are formed. Dark suboxide rows are also observed (oval).

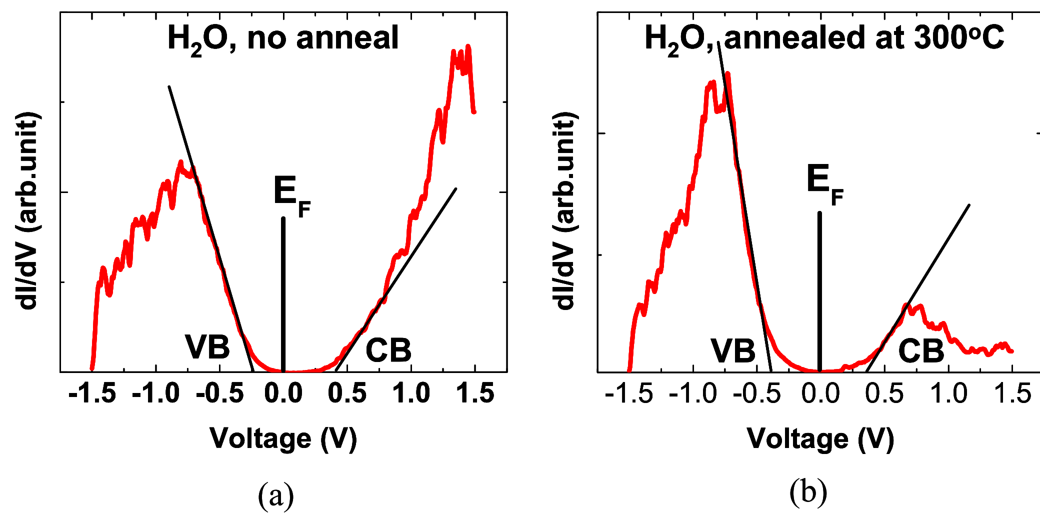

Figure 3.2 STS of H_2O/Ge(100) before and after post deposition annealing. (a) STS of H_2O dosed Ge(100) at room temperature. The Fermi level of *n*-type Ge surface is pinned near the valence band edge. (b) STS of H_2O dosed Ge(100) annealed at 300°C. The Fermi level of *n*-type Ge surface is pinned near the midgap.

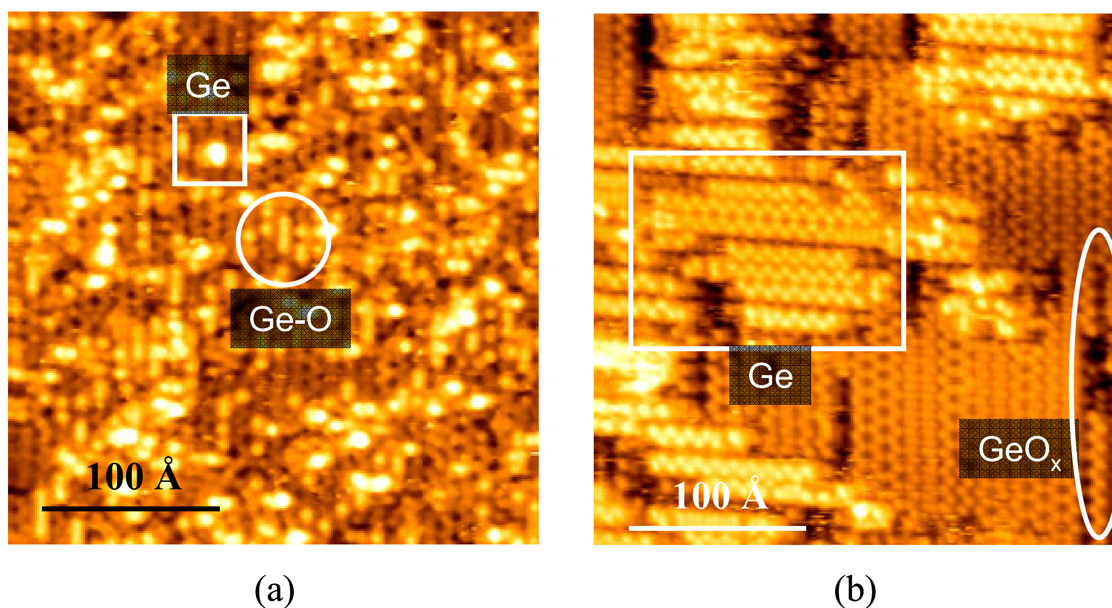

Figure 3.3 STM of ebeam GeO_2 on Ge(100) before and after post deposition annealing. (a) Ge(100) surface deposited with GeO_2 at room temperature. Semi-ordered Ge-O structures (circle) and Ge ad-atoms (square) are observed. (b) Ge(100) surface deposited with GeO_2 after annealing at 325°C. Ge regrowth island (rectangle) and suboxide rows (oval) are shown.

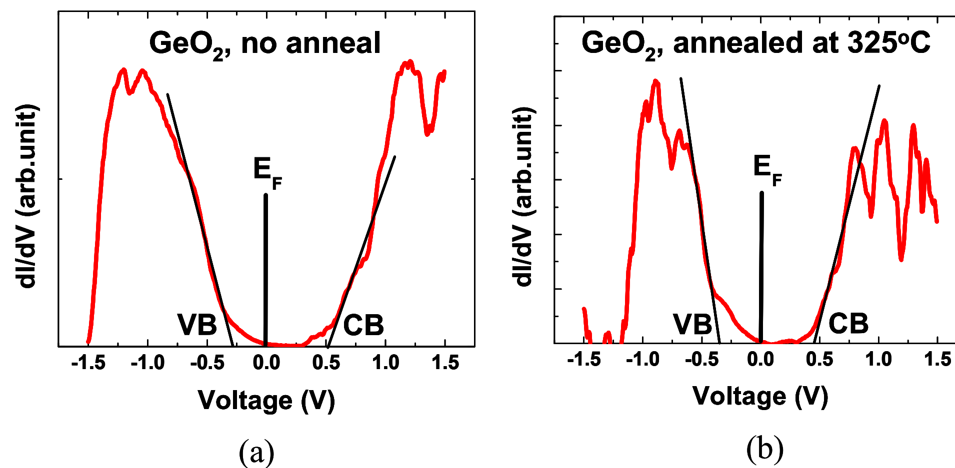

Figure 3.4 STS of e-beam GeO_2 on Ge(100) before and after post deposition annealing. (a) STS of GeO_2 deposited Ge(100) at room temperature. The Fermi level of *n*-type Ge surface is pinned near the valence band edge. (b) STS of GeO_2 deposited on Ge(100) after annealing at 325°C. The Fermi level of *n*-type Ge surface is pinned near the valence band edge.

3.8 References

[1] B. DeJaeger, et al., Microelectron. Eng. 80 (2005) 26.

[2] T. Maeda, S. Takagi, T. Ohnishi, M. Lippmaa, Mat. Sci. Semicon. Proc. 9 (2006) 706.

[3] R. Xie, M. Yu, M.Y. Lai, L. Chan, C. Zhu, Appl. Phys. Lett. 92 (16) (2008) 163505.

[4] H. Kim, P.C. McIntyre, C.-O. Chui, K.C. Saraswat, M.-H. Cho, Appl. Phys. Lett. 85 (14) (2004) 2902.

[5] T. Maeda, T. Yasuda, M. Nishizawa, N. Miyata, Y. Morita, S. Takagi, J. Appl. Phys. 100 (1) (2006) 014101.

[6] Y. Oshima, Y. Sun, D. Kuzum, T. Sugawara, K.C. Saraswat, P. Pianetta, P.C. McIntyre, J. of Electrochem. Soc. 155 (12) (2008) G304-G309.

[7] F. Bellenger, M. Houssa, A. Delabie, V. Afanasiev, T. Conard, M. Caymax, M. Meuris, K. DeMeyer, M.M. Heyns, J. of Electrochem. Soc. 155 (2) (2008) G33-G38.

[8] A. Delabie, F. Bellenger, M. Houssa, T. Conard, S. VanElshocht, M. Caymax, M. Heyns, M. Meuris, Appl. Phys. Lett. 91 (8) (2007) 082904.

[9] D. Kuzum, T. Krishnamohan, A.J. Pethe, A.K. Okyay, Y. Oshima, Y. Sun, J.P. McVittie, P.A. Pianetta, P.C. McIntyre, K.C. Saraswat, IEEE Elec. Dev. Lett. 29 (4) (2008) 328.

[10] C.H. Lee, T. Tabata, T. Nishimura, K. Nagashio, K. Kita, A. Toriumi, ECS Trans. 19 (1) (2009) 165-173.

[11] H. Matsubara, T. Sasada, M. Takenaka, S. Takagi, Appl. Phys. Lett. 93 (3) (2008) 032104.

[12] T. Maeda, M. Nishizawa, Y. Morita, S. Takagi, Appl. Phys. Lett. 90 (7) (2007) 072911.

[13] S.J. Wang, J.W. Chai, J.S. Pan, A.C.H. Huan, Appl. Phys. Lett. 89 (2) (2006) 022105.

[14] T.J. Grassman, S.R. Bishop, A.C. Kummel, Surf. Sci. 602 (14) (2008) 2373-2381.

[15] S.J. Jung, J.Y. Lee, S. Hong, S. Kim, J. Phys. Chem. B 109 (51) (2005) 24445-24449.

[16] S. Shimokawa, A. Namiki, M.N.-Gamo, T. Ando, J. Chem. Phys. 113 (2000) 6916.

[17] Y. Barta, D. Kabiraj, D. Kanjilal, Solid State Commun. 143 (2007) 213.

[18] M. Ardyanian, H. Rinnert, X. Devaux, M. Vergnat, Appl. Phys. Lett. 89 (2006) 011902.

[19] K. Prabhakaran, F. Maeda, Y. Watanabe, T. Ogino, Thin Solid Films 369 (1-2) (2000) 289-292.

CHAPTER FOUR

Effect of H_2O Chemisorption on Passivation of Ge(100) Surface

4.1 Abstract

The effect of chemisorption of H_2O on the atomic and electronic structures of a Ge(100) surface was investigated using scanning tunneling microscopy (STM) and scanning tunneling spectroscopy (STS). With a saturation H_2O dose at room temperature (RT), a highly-ordered structure, due to the dissociative chemisorption of H_2O, was observed on a Ge(100) surface with a coverage of 0.85 monolayers (ML). Annealing the room temperature H_2O-dosed Ge surface over 100°C decreased the coverage of H_2O to 0.6 ML at 175°C. Further annealing at 250°C decreased the coverage of H_2O sites to 0.15 ML, and the surface reconstruction of Ge dimers was observed over much of the surface. Annealing above 300°C induced Ge suboxide structures, similar to the oxygen-dosed Ge surface. STS measurements confirmed that the surface states near Fermi energy are removed by the H_2O chemisorption as the dangling bonds of Ge atoms are terminated by –OH and –H. The H_2O pre-dose at room temperature provides a template for the ultrathin passivation of Ge(100) surface via atomic layer deposition (ALD) at RT, since near monolayer nucleation can be obtained with a ½ hydroxylated and ½ hydrogenated Ge surface.

4.2 Introduction

Germanium has drawn a significant interest as a new channel material of the metal-oxide-semiconductor field effect transistor (MOSFET) because it has superior electronic properties such as high electron and hole mobility compared to silicon. By integrating high-k dielectric materials as a gate oxide layer, Ge-channel MOSFETs are expected to exceed the performance of conventional Si-channel devices. However, the high interface trap density between a Ge and a high-k dielectric layer is a challenging issue in fabricating Ge-based MOSFETs because the channel mobility is severely affected by the interface quality [1-3]. To reduce the interface trap density, a passivation process is required that can minimize the dangling bonds of the Ge surface atoms.

Many passivation methods for Ge surfaces have been proposed [4-10], and two different approaches have been intensively studied – nitridation [11-13] and oxidation [14-18]. Nitridation of the Ge surface is typically performed using a plasma source to produce a thermally stable Ge oxynitride or Ge nitride layer in order to suppress the out-diffusion of GeO from the Ge surface into the high-k dielectric layer during the post-deposition annealing process [19,20]. Oxidation using ozone or high pressure O_2 is also found to passivate the Ge surface by forming a stoichiometric GeO_2 layer which minimizes the suboxide species at the interface. However, to scale down the equivalent oxide thickness (EOT) of the Ge-channel MOSFET device, the thickness of these passivation layers has to be reduced to about one monolayer (ML).

In previous work, monolayer passivation using nitridation and oxidation was investigated at an atomic level using scanning tunneling microscopy (STM) [21-23]. An ordered Ge subnitride structure was observed on a Ge(100) surface after plasma nitridation at 500°C, which confirmed the thermal stability of the subnitride at this temperature. However, scanning tunneling spectroscopy (STS) measurements and density functional theory (DFT) calculations showed that this ordered subnitride structure pins the Fermi level of a n-type Ge surface near the valence band edge due to the increase of dangling bonds and the subsurface strain. A further process, such as H-passivation, is required to remove the density of states near the Fermi energy from the Ge subnitride structure [21]. Monolayer oxidation using gaseous oxygen or e-beam evaporation of GeO_2 was also studied, but both oxidants produced Ge ad-atoms which caused Fermi level pinning on the surface at RT [22,23]. Moreover, the stoichiometry of GeO_2 was not maintained due to the instability of GeO_2 on a Ge surface ($GeO_2 + Ge \rightarrow 2GeO$) [24], causing the formation of Ge suboxides at temperatures over 300°C consistent with observation of the Fermi level pinning [22,23].

Recently, Swaminathan et al. reported the H_2O pre-pulsing on a Ge(100) surface improved the interface quality between a Ge surface and a Al_2O_3 layer during atomic layer deposition (ALD) [25]. It was proposed that some of the defect states are passivated by hydroxylating Ge atoms in the interface layer using multiple cycles of H_2O pulsing at 250°C. Since H_2O is a commonly used oxygen precursor for the ALD process and wet oxidation [26-28], it is likely to be a very practical method to passivate a Ge surface. To optimize the H_2O passivation process, a method must be developed which does not disrupt the surface.

In this paper, the chemisorption of H_2O at a high coverage and its effect on the electronic structure of a Ge(100) surface were studied using controlled dosing of H_2O. To investigate the temperature dependence of H_2O chemisorption on a Ge(100) surface, the structure of a H_2O dosed Ge surface was examined with *in situ* analysis performed with STM at different annealing temperatures. The surface electronic states related to the H_2O chemisorption were probed using *in situ* STS measurements.

4.3 Experimental details

Two different ultrahigh vacuum (UHV) systems were employed for this study. The low coverage H_2O dosing at RT and 250°C were performed in a UHV system equipped with a sputter gun (EX05, VG Microtech), a differentially-pumped H_2O dosing system, and a STM (Autoprobe VP1, Park Scientific Instrument). The high coverage H_2O dosing at RT and the thermal annealing experiments were performed in a second system with a sputter gun (Model-1403, Nonsequitur Technologies), a differentially-pumped H_2O dosing module, and a STM (LT-STM, Omicron Nanotechnology).

An epitaxial grade n-type Ge(100) wafer (Sb-doped, 0.005-0.020 Ωcm, Wafer World Inc.) was cut in a small piece (12.5 mm × 4.5 mm) and ultrasonicated with acetone, methanol, and deionized water to degrease the surface. After transfer into the UHV chamber, the Ge samples were sputtered by an Ar^+ ion beam at 500°C for 30 minutes and subsequently annealed at 700°C for 20 minutes. An atomically flat Ge(100) surface was obtained after several cycles of the sputter-anneal process, which was confirmed by STM and STS measurements.

The pure H_2O (HPLC grade) vapor was introduced to the sample at RT through a clean dosing line by controlling the flow rate of the vapor using a needle valve. Exposure of H_2O was estimated in Langmuirs (1 L = 1×10^{-6} Torr s). For a high coverage H_2O (4×10^{6} L) and annealing experiment, water vapor was dosed onto the clean Ge(100) surface in the separate load-lock with a base pressure of 5×10^{-9} Torr, and transferred back into the preparation chamber. Thermal annealing of a H_2O dosed sample was performed in the preparation chamber with base pressure of 2×10^{-10} Torr by directly heating the sample while monitoring the surface temperature using a pyrometer. After H_2O dosing and annealing, the sample was transferred *in situ* to the STM chamber at a base pressure of 2×10^{-11} Torr.

The atomic resolution STM images were obtained using the constant-current mode STM (I_{sp} = 0.2 nA) with an electrochemically etched tungsten tip. The sample bias was applied at -1.8 to -2.0 V for a filled-state STM imaging, and +1.5 to +2.0 V for an empty-state imaging. To investigate the electronic structure of the surface, STS measurements were carried out using a variable-z method with a modulation signal (0.1 V, 650 Hz) from an external lock-in amplifier, while sweeping the sample bias from -1.5 to +1.5 V.

4.4 Results and discussion

A clean and atomically flat Ge(100) surface was obtained with multiple cycles of sputtering and annealing. Figure 4.1(a) shows a typical filled-state STM image of a clean Ge(100) surface consisting of the c(4×2) and (2×1) dimer reconstructions. After a 100 L H_2O dose at RT, 0.2 ML of dark regions were formed on the Ge(100) surface as shown in Figure 4.1(b). The dark regions observed on this image are attributed to the H_2O chemisorption sites, consistent with the results reported by Jung et al [29]. It was proposed that the dissociative chemisorption of H_2O terminates the dangling bonds on a Ge dimer with –OH and –H, which creates a H-Ge-Ge-OH configuration [29]. This bonding configuration eliminates the surface states near the Fermi energy due to Ge dangling bonds and results in a lower tunneling current on the H_2O chemisorption sites making them darker than the bare Ge dimers in the STM images consistent with extensive studies on H_2O/Si(100) [30]. In Figure 4.1(b), the dark H_2O chemisorbed dimers are exactly aligned along the bright bare Ge dimer rows. The images show that the H_2O sites readily form an ordered submonolayer island at RT without disturbing Ge surface atoms. This is a significant difference from the case of the O_2 dosed Ge surface which produces discrete O displacement sites and Ge adatoms with the same densities [23]. Oxygen induced Ge ad-species, which are easily identified by their typical height (1.2 – 1.4 Å above the surface) [23], are not observed on the H_2O dosed Ge(100) surface.

The low coverage results suggest that each Ge dimer might be terminated with one -OH and one –H with a sufficiently high H_2O dose at RT. To the authors' knowledge,

STM and STS studies of a Ge surface with a high coverage of H_2O have not been reported. Figure 4.2(a) shows the filled-state STM image of a Ge(100) surface dosed with 4×10^6 L of H_2O at RT with the diagrams of surface structures at corresponding positions. A majority of the surface (0.85 ML) is covered by the dark H_2O chemisorption sites, which are well-resolved in the blue box in Figure 4.2(a). On each H_2O-chemisorbed dimer, two separate protrusions are observed indicating –OH and –H terminations of the dangling bonds on the dimer. In addition, some of those dimers show a slight difference in brightness between the two protrusions, possibly reflecting the different electron density between –OH and –H terminations. STM simulation with density functional theory suggests the –OH bonding site should be slightly brighter than the –H bonding site in the filled state image [29].

Besides the high coverage H_2O sites, Figure 4.2(a) shows fuzzy bright sites randomly distributed on the surface. Similar features were also observed on H_2O or H_2 saturated Si(100) surfaces [30,31]. These features are attributed to single (Fig 2(a), green box) or double (Fig 2(a), red box) dangling bond sites. Single dangling bond (sDB) sites are typically found to be on one side of the dimer row, indicating the other side of the dimer is still bonded to –OH or –H. On the contrary, double dangling bond (dDB) sites are found to be centered on the dimer row due to their symmetric geometry. The existence of these unreacted double dangling bond sites, even with relatively high exposure of H_2O (> 1×10^6 L) indicates the desorption of H_2O occurring on Ge(100) surface at RT during the adsorption of H_2O. Papagno et al. showed that H_2O does not adsorb easily on Ge(100) at room temperature, but the adsorption is enhanced when the sample is cooled down at liquid nitrogen temperature [32]. Therefore, to achieve a

completely full monolayer of H_2O chemisorption, a cryogenic H_2O dosing at low temperature might be required, as proven in the case of H_2O on Si(100) [33,34]. However, the current results clearly show that almost one monolayer of Ge-H and Ge-OH chemisorption sites can be formed on clean Ge(100) without disrupting the interface by dosing with H_2O at RT, which is in clear contrast to dosing with N or O_2 [21,23].

To further investigate the electronic structure of H_2O dosed Ge(100) surface, STS measurements were performed on H_2O chemisorption sites, single dangling bond sites, and double dangling bond sites. Figure 4.2(b) compares the STS curves measured from each of these surface species. It was found that both of the sDB and dDB sites have energy states near 0.5 eV consistent with the presence of dangling bonds. Conversely, on the H_2O sites, the energy states around 0.5 eV are significantly reduced showing that the dangling bond states are removed by the –OH and –H bonds. This again is in clear contrast to dosing with O_2, N, and GeO_2 where it is impossible to passivate the surface using these passivants due to the formation of Ge adatoms [21-23].

Although there are several reports of STM studies on H_2O dosed Si(100) surface and H_2O dose at low coverage onto Ge(100) at RT [29,30], the temperature dependence of the H_2O chemisorption at any coverage onto Ge(100) surface has not been studied by STM. To investigate the thermal behavior of the H_2O chemisorbed species, the RT H_2O dosed sample was annealed at 100, 175, 250, and 300°C for 5 minutes. Figure 4.3 shows the STM images obtained from the Ge(100) surface H_2O dosed at RT and annealed at 100 and 175°C. The coverage of dark H_2O sites decreases from 0.85 ML at RT to 0.6 ML at 175°C, indicating the recombinative desorption of H_2 or H_2O.

The desorption of H_2 or H_2O gradually restores the clean surface reconstructions of Ge dimers in isolated regions. With a 250°C anneal (Figure 4.4), most of the Ge surface reconstruction is recovered, and the coverage of H_2O sites significantly decreases to 0.15 ML. Additionally, two types of bright sites appear on the surface, denoted as 'A' and 'B' in Figure 4.4. Bright site A is located in between the Ge dimer rows, usually appearing in a group lining up perpendicular to the dimer row direction. On the contrary, bright site B is centered on the dimer row, normally appearing by itself. A significant change of H_2O coverage and the appearance of bright sites at 250°C is consistent with previous studies on the thermal reactions of H_2O on Ge(100) [32,35,36]. A temperature programmed desorption (TPD) experiment [35] showed that -OH and –H recombination readily occurs above 200°C, consistent with a large reduction of H_2O sites between 175°C and 250°C observed in the present study. Moreover, the TPD data was consistent with the hydroxyl group starting to dissociate at 180°C [32] to produce atomic O species consistent with the observation of bright sites in the present STM study of 250°C annealed surfaces. The O adsorption site atop of a Ge dimer is observed as a slightly bright site in the filled state STM image [23,37]. In the same manner, O atoms bridging two adjacent Ge dimers also can appear as bright features in the STM image. Figure 4.5 illustrates two different pathways for formation of these atomic O structures via hydroxyl dissociation. Two H atoms, one dissociated from a hydroxyl and one from a Ge dimer, will recombine and desorb as a hydrogen molecule. When the recombination takes place between adjacent Ge dimers, O bridging sites will be formed (bright site A). Conversely, if the recombination occurs within a dimer, an O adsorption site will be formed (bright

site B). Since the H_2O recombinative desorption is still the major reaction at this temperature [35], the coverage of these bright sites is low.

Further annealing at 300°C produced Ge suboxide rows on H_2O-dosed Ge(100), similar to the suboxide rows observed on the O_2-dosed Ge(100) annealed at the same temperature [23] (Figure 4.6). Hydrogen atoms are desorbed at this temperature as H_2 molecules [36,38]; therefore, the surface is essentially the same as an O_2-dosed and annealed Ge(100) surface. It is likely the remaining O species convert to the O dimer displacement sites, and these site coalesce into the suboxide rows appearing as a dark row on the STM image [23]. The O displacement produces Ge ad-atoms, but at this temperature the Ge ad-species will diffuse away to the step edges [23], accounting for the absence of Ge ad-atoms on the surface.

The low coverage of H_2O chemisorption and the hydroxyl dissociation at 250°C can clearly explain the multiple H_2O pre-pulsing experiments reported by Swaminathan et al [25]. The H_2O pre-dose on a Ge(100) surface prior to the ALD process is expected to enhance the initial ALD reaction for precursors with methyl groups (e.g. trimethylaluminum (TMA)) by providing hydroxyl groups on the surface. However, due to the high desorption rate of H_2O on a Ge(100) at 250°C, a large exposure of H_2O would be required to maximize the hydroxyl coverage by creating a multilayer $Ge_xO_y(OH)_z$ on the surface, consistent with multiple cycles of H_2O prepulsing.

While the H_2O chemisorption is shown to passivate the Ge surface effectively by terminating dangling bonds without disturbing surface Ge atoms (Figure 4.2), the coverage of H_2O is severely limited at elevated temperatures. In addition, the oxygen structures due to the –OH dissociation and hydrogen desorption at 250°C (Figures 3.4 and

3.5) are less desired for the ALD process than the –OH and –H sites because the dissociative chemisorption should be most favorable for –OH sites since they can form a Ge-O-Metal bond while providing a hydrogen atom to the organic ligand to aid in desorption. Therefore, it is necessary to utilize the H_2O chemisorbed Ge surface at RT to maximize its coverage and H-Ge-Ge-OH configuration. It is proposed that the –OH and –H functionalized Ge surface at RT serves as a template for monolayer nucleation during the first cycle of ALD. By providing the metal precursor such as TMA on the H_2O dosed surface at RT, a saturation layer of stable Ge-O-Al bonds will be formed while preserving the high coverage of H_2O and a nearly perfect monolayer passivation is expected to form on a Ge(100) surface [39].

4.5 Conclusions

A controlled dose of H_2O was performed on an atomically flat Ge(100) surface and the topographic and electronic surface structures at a high H_2O coverage were investigated using STM/STS. With a 4×10^6 L of H_2O dosing on a Ge(100) surface at RT, the ordered H_2O chemisorption structures were formed on the surface at a coverage of 0.85 ML without disrupting the surface Ge atoms. The fuzzy bright structures observed on the high coverage H_2O dosed Ge surface were isolated dangling bonds, which were confirmed by the STS measurement. STS measurements also showed that the –OH and –H termination of a Ge surface dimer removed the density of states due to the dangling bonds.

By annealing the RT H_2O dosed surface at 250^oC, the coverage of H_2O sites decreased to 0.15 ML, demonstrating the desorption of H_2O. To utilize the nature of –OH and –H in the initial ALD process, it is proposed to perform the H_2O dose at low temperature which can also minimize the formation of isolated dangling bonds. A full monolayer containing ½ ML of –OH and ½ ML of –H is expected to serve for an ideal passivation of Ge(100) surface combined with a methyl-containing ALD precursor at RT.

4.6 Acknowledgements

This work is supported by the MSD Focus Center Research Program (2051.001). The authors would like to acknowledge Prof. Krishna Saraswat and Prof. Paul McIntyre for their helpful discussions.

Chapter 4, in full, has been submitted for publication of the material as it may appear in J.S. Lee, T. Kaufman-Osborn, W. Melitz, S. Lee and A.C. Kummel, 'Effect of H_2O Chemisorption on Passivation of Ge(100) Surface studied by Scanning Tunneling Microscopy', *Surface Science* (2011). The dissertation author was the primary investigator and author of this paper.

4.7 Figures

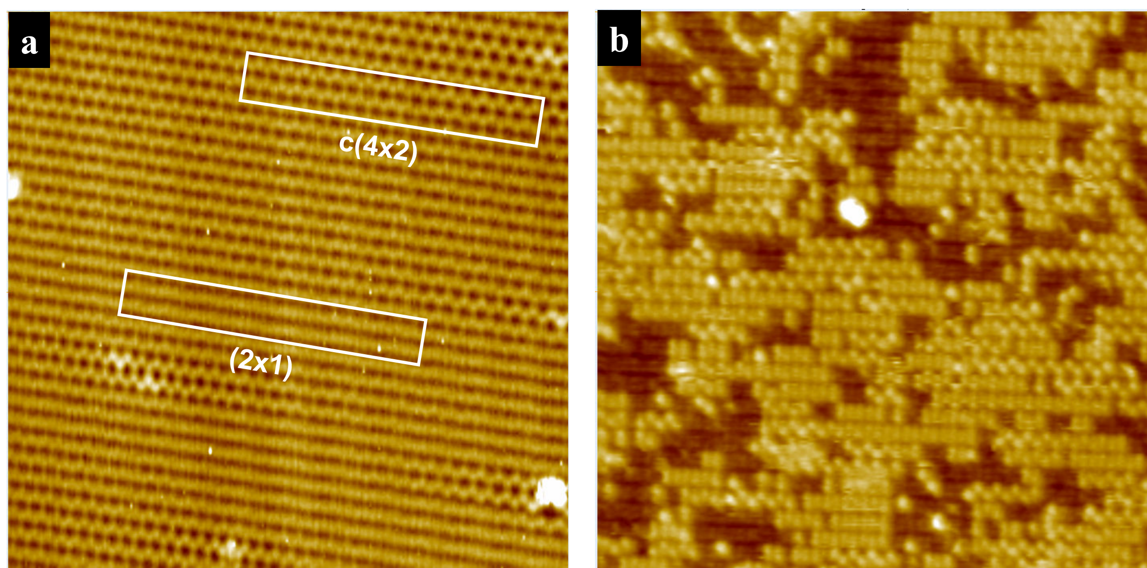

Figure 4.1 Filled state STM images (30×30 nm^2, Vs = -2.0 V, It = 0.2 nA) of a clean Ge(100) surface (a), and a 100 L H_2O dosed Ge(100) (b). (a) A clean Ge(100) surface consists of (2×1) and c(4×2) dimer reconstructions. (b) A 100 L H_2O dose at RT produces 0.2 ML of H_2O chemisorption sites (dark regions) on a Ge(100) surface.

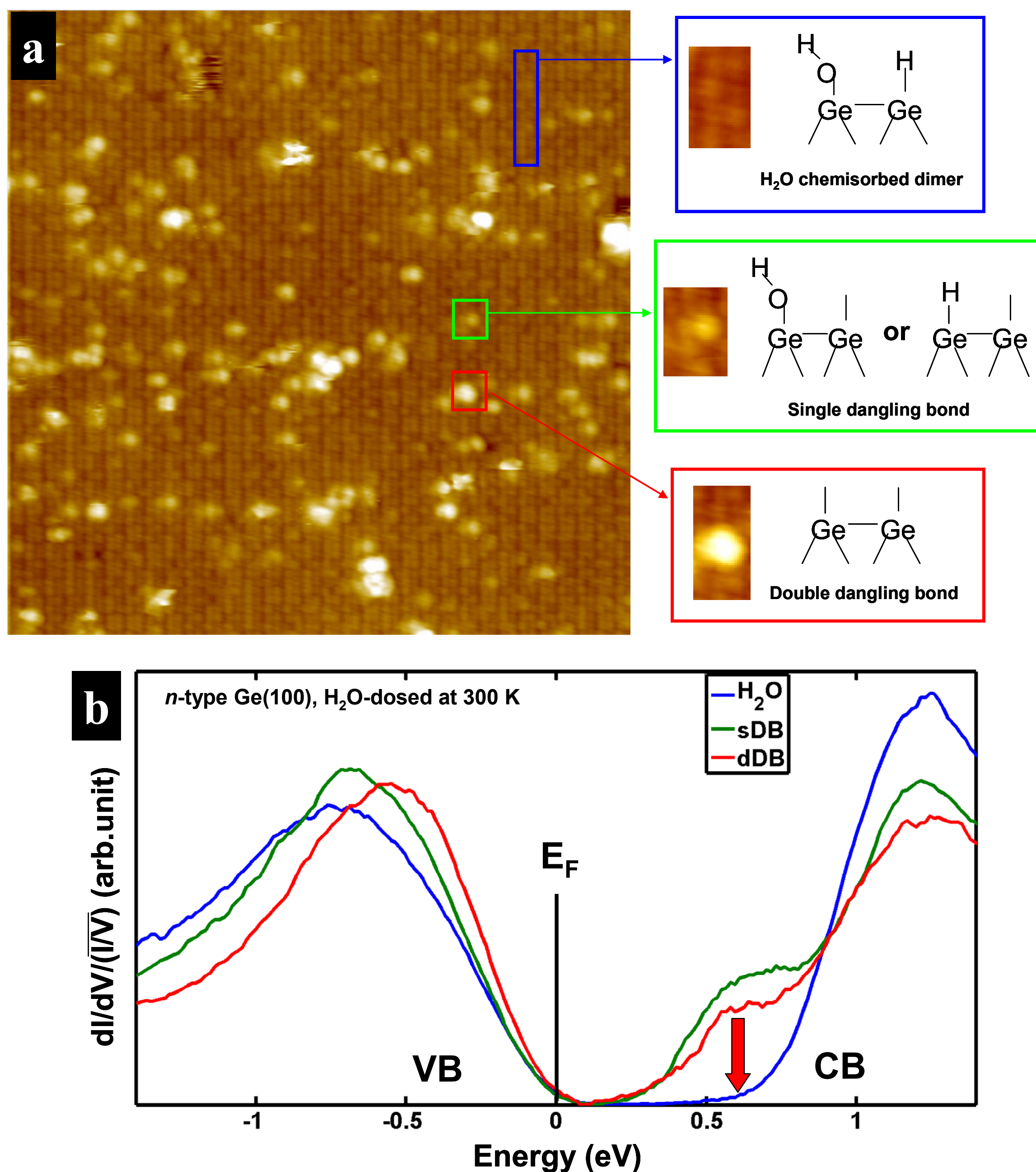

Figure 4.2 STM and STS results of a H_2O dosed Ge(100) surface (4×10^6 L) at RT. (a) Filled state STM image (30×30 nm^2, Vs = -1.8 V, It = 0.2 nA) shows 0.85 ML of a Ge surface is covered by H_2O chemisorption. H_2O sites (blue box), single (green box) and double (red box) dangling bond sites are denoted with enlarged images and schematic diagrams. (b) STS measured on H_2O sites (blue curve) shows reduction of dangling bond states (red arrow) compared with single and double dangling bonds (green and red curves).

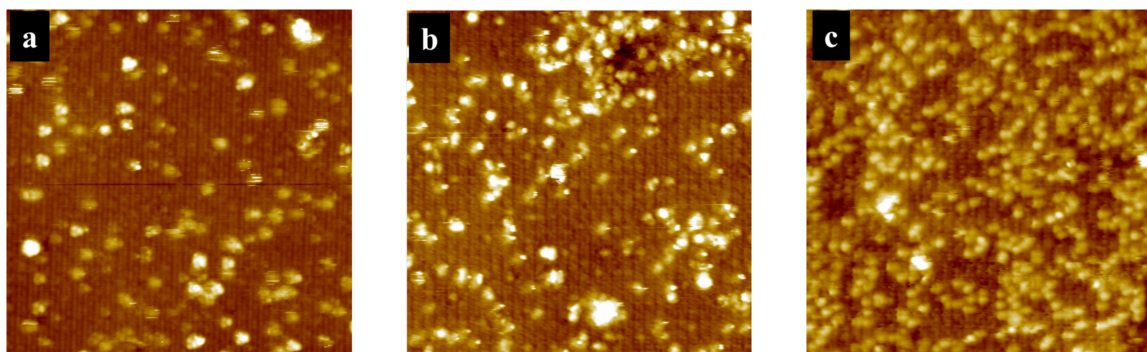

Figure 4.3 STM images (30 × 30 nm^2, Vs = -1.8 V, It = 0.2 nA) of annealing experiments of a H_2O-dosed Ge(100) surface. (a) H_2O-dosed at RT, non-annealed Ge(100) surface. H_2O coverage is 0.85 ML. (b) Annealed at 100°C for 5 min. H_2O coverage is 0.8 ML. (c) Annealed at 175°C for 5 min. H_2O coverage is 0.6 ML

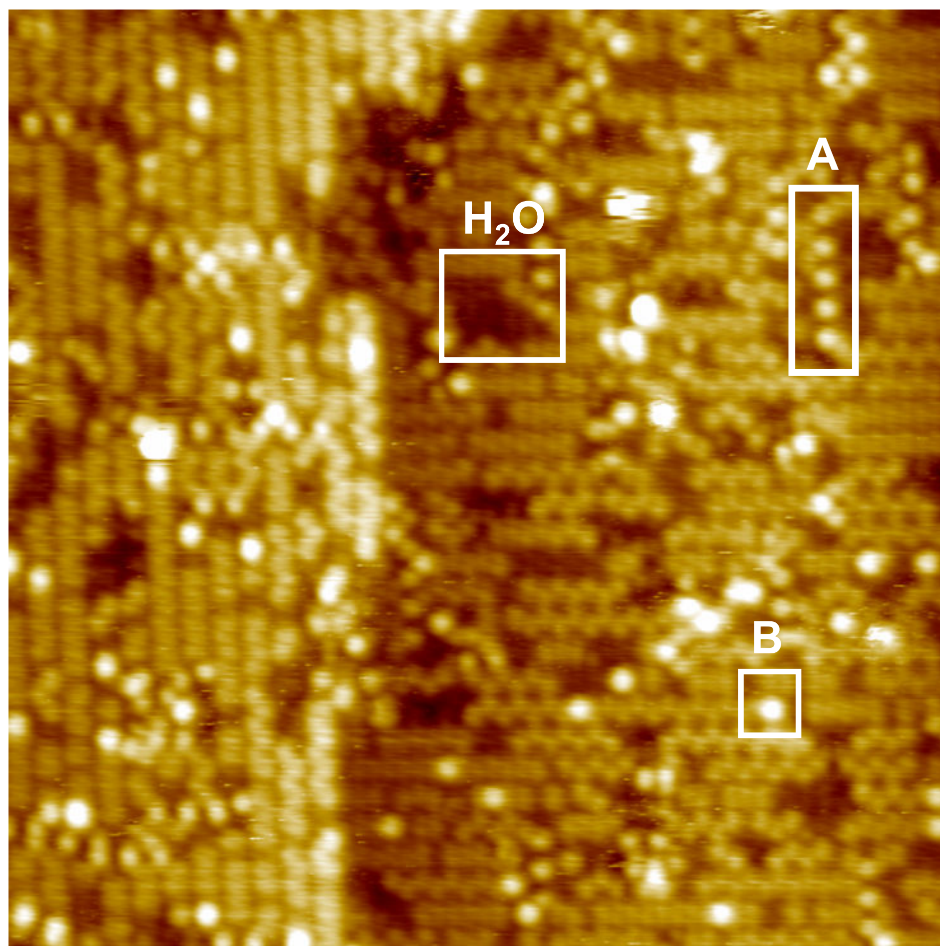

Figure 4.4 Filled state STM image (30 × 30 nm^2, Vs = -1.8 V, It = 0.2 nA) of a Ge(100) surface H_2O-dosed at RT and annealed at 250°C for 5 minutes. The coverage of H_2O sites decreased to 0.15 ML. Two different kinds of bright sites are observed on the trough (marked as A) and on the row (marked as B).

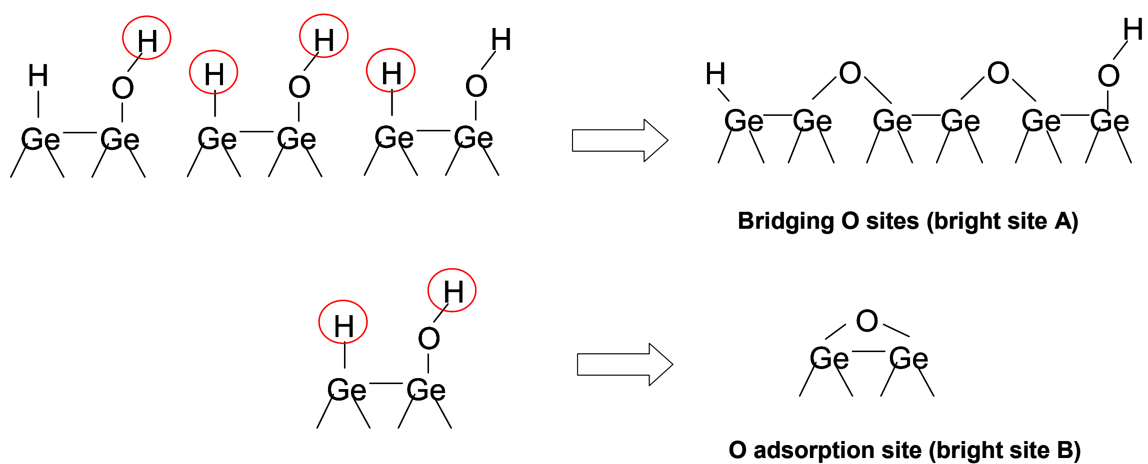

Figure 4.5 Schematic diagrams of two pathways of H_2 desorption on the H_2O-dosed Ge(100) surface. H atoms marked with red circles are recombined and desorbed as H_2. As a result, bridging O sites (corresponding bright site A in Fig 4) and O adsorption site (corresponding bright site B in Fig 4) are produced.

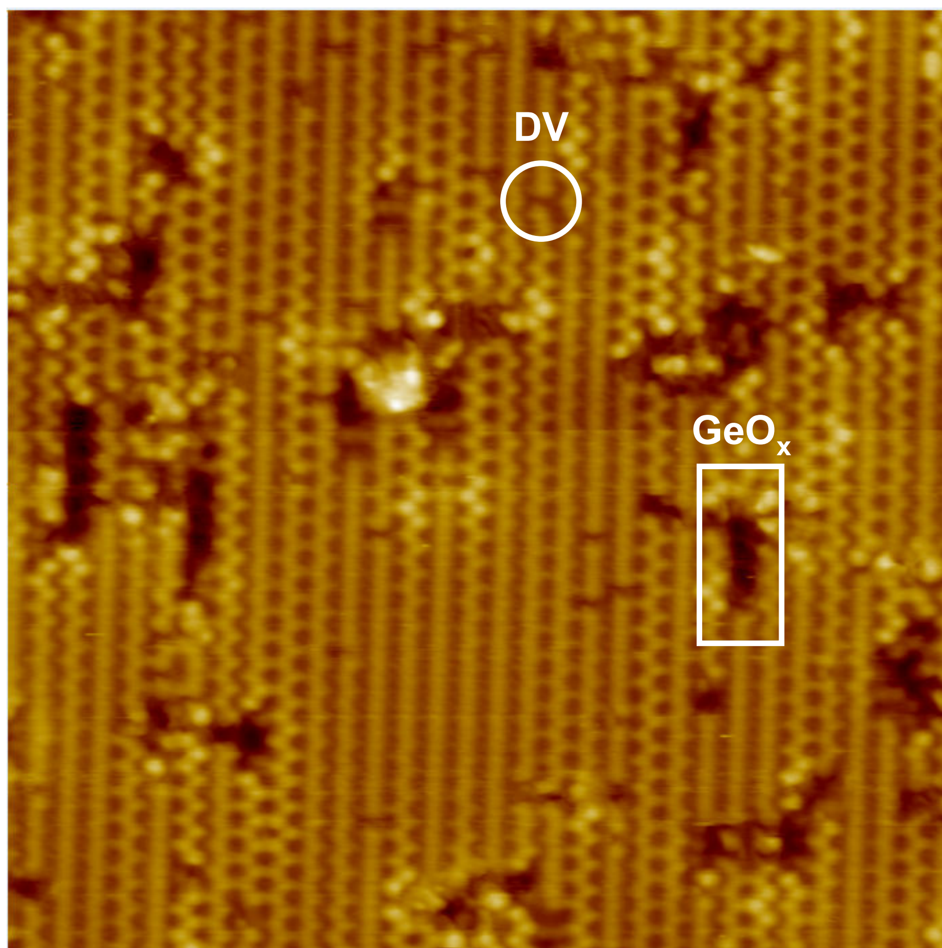

Figure 4.6 Filled state STM image (30 × 30 nm^2, Vs = -1.8 V, It = 0.2 nA) of a Ge(100) surface H_2O-dosed at RT and annealed at 300°C for 5 minutes. Dimer vacancies (marked as DV) and Ge suboxide rows (marked as GeO_x) are observed.

4.8 References

[1] J. Mitard, et al., Symp. VLSI Tech. Dig. (2009) 82-83.

[2] D. Kuzum, T. Krishnamohan, A. Nainani, Y. Sun, P.A. Pianetta, H.-S.P. Wong, K.C. Saraswat, IEEE Trans. Elect. Dev. 58 (1) (2011) 59-66.

[3] T. Maeda, Y. Morita, S. Takagi, Symp. VLSI Tech. Dig. (2010) 213-214.

[4] B. DeJaeger, et al., Microelectron. Eng. 80 (2005) 26.

[5] N. Taoka, M. Harada, Y. Yamashita, T. Yamamoto, N. Sugiyama, S.-i. Takagi, Appl. Phys. Lett. 92 (11) (2008) 113511.

[6] R. Xie, M. Yu, M.Y. Lai, L. Chan, C. Zhu, Appl. Phys. Lett. 92 (16) (2008) 163505.

[7] P. Ardalan, E.R. Pickett, J.S. Harris, Jr., A.F. Marshall, S.F. Bent, Appl. Phys. Lett. 92 (25) (2008) 252902.

[8] S. Sun, Y. Sun, Z. Liu, D.-I. Lee, P. Pianetta, Appl. Phys. Lett. 89 (23) (2006) 231925.

[9] T. Maeda, S. Takagi, T. Ohnishi, M. Lippmaa, Mat. Sci. Semicon. Proc. 9 (2006) 706.

[10] R. Xie, C. Zhu, IEEE Elec. Dev. Lett. 28 (2007) 976.

[11] H. Kim, P.C. McIntyre, C.-O. Chui, K.C. Saraswat, M.-H. Cho, Appl. Phys. Lett. 85 (14) (2004) 2902.

[12] T. Sugawara, R. Sreenivasan, P.C. McIntyre, J. Vac. Sci. Technol. B 24 (5) (2006) 2442.

[13] T. Maeda, T. Yasuda, M. Nishizawa, N. Miyata, Y. Morita, S. Takagi, J. Appl. Phys. 100 (1) (2006) 014101.

[14] F. Bellenger, M. Houssa, A. Delabie, V. Afanasiev, T. Conard, M. Caymax, M. Meuris, K. DeMeyer, M.M. Heyns, J. of Electrochem. Soc. 155 (2) (2008) G33-G38.

[15] A. Delabie, F. Bellenger, M. Houssa, T. Conard, S. VanElshocht, M. Caymax, M. Heyns, M. Meuris, Appl. Phys. Lett. 91 (8) (2007) 082904.

[16] D. Kuzum, T. Krishnamohan, A.J. Pethe, A.K. Okyay, Y. Oshima, Y. Sun, J.P. McVittie, P.A. Pianetta, P.C. McIntyre, K.C. Saraswat, IEEE Elec. Dev. Lett. 29 (4) (2008) 328.

[17] C.H. Lee, T. Tabata, T. Nishimura, K. Nagashio, K. Kita, A. Toriumi, ECS Trans. 19 (1) (2009) 165-173.

[18] H. Matsubara, T. Sasada, M. Takenaka, S. Takagi, Appl. Phys. Lett. 93 (3) (2008) 032104.

[19] T. Maeda, M. Nishizawa, Y. Morita, S. Takagi, Appl. Phys. Lett. 90 (7) (2007) 072911.

[20] S.J. Wang, J.W. Chai, J.S. Pan, A.C.H. Huan, Appl. Phys. Lett. 89 (2) (2006) 022105.

[21] J.S. Lee, S.R. Bishop, T.J. Grassman, A.C. Kummel, Surf. Sci. 604 (15-16) (2010) 1239-1246.

[22] J.S. Lee, S.R. Bishop, T. Kaufman-Osborn, E. Chagarov, A.C. Kummel, ECS Trans. 33 (6) (2010) 447-454.

[23] T.J. Grassman, S.R. Bishop, A.C. Kummel, Surf. Sci. 602 (14) (2008) 2373-2381.

[24] K. Prabhakaran, F. Maeda, Y. Watanabe, T. Ogino, Thin Solid Films 369 (1-2) (2000) 289-292.

[25] S. Swaminathan, Y. Oshima, M.A. Kelly, P.C. McIntyre, Appl. Phys. Lett. 95 (3) (2009) 032907.

[26] R. Puurunen, J. Appl. Phys. 97 (12) (2005) 121301.

[27] N. Sano, M. Sekiya, M. Hara, A. Kohno, T. Sameshima, Appl. Phys. Lett. 66 (16) (1995) 2107.

[28] M.K. Weldon, B.B. Stefanov, K. Raghavachari, Y.J. Chabal, Phys. Rev. Lett. 79 (15) (1997) 2851.

[29] S.J. Jung, J.Y. Lee, S. Hong, S. Kim, J. Phys. Chem. B 109 (51) (2005) 24445-24449.

[30] L. Andersohn, U. Köhler, Surf. Sci. 284 (1-2) (1993) 77-90.

[31] J.J. Boland, Phys. Rev. Lett. 67 (12) (1991) 1539.

[32] L. Papagno, D. Frankel, Y. Chen, L.S. Caputi, J. Anderson, G.J. Lapeyre, Surf. Sci. 248 (3) (1991) 343-348.

[33] H.S. Kato, K. Akagi, S.Tsuneyuki, M. Kawai, J. Phys. Chem. C 112 (33) (2008) 12879-12886.

[34] D.B. Skliar, B.G. Willis, J. Phys. Chem. C 112 (25) (2008) 9434-9442.

[35] T.-F. Teng, W.-L. Lee, Y.-F. Chang, J.-C. Jiang, J.-H. Wang, W.-H. Hung, J. Phys. Chem. C 114 (2) (2010) 1019-1027.

[36] J.Y. Lee, J.Y. Maeng, A. Kim, Y.E. Cho, S. Kim, J. Chem. Phys. 118 (4) (2003) 1929.

[37] T. Fukuda, T. Ogino, Phys. Rev. B 56 (20) (1997) 13190.

[38] J.Y. Maeng, J.Y. Lee, Y.E. Cho, S. Kim, Appl. Phys. Lett. 81 (19) (2002) 3555.

[39] J.S. Lee, T. Kaufman-Osborn, W. Melitz, S. Lee, A.C. Kummel, (in preparation).

CHAPTER FIVE

Nucleation of Trimethylaluminum on Clean and H_2O dosed Ge(100) Surfaces

5.1 Abstract

The direct reaction of trimethyl aluminum (TMA) on a Ge(100) surface and the effect of monolayer H_2O pre-dosing were investigated using scanning tunneling microscopy (STM), scanning tunneling spectroscopy (STS), and x-ray photoelectron spectroscopy (XPS). At room temperature (RT), a saturation TMA dose produced 0.8 monolayer (ML) of semi-ordered species on a Ge(100) surface due to the dissociative chemisorption of TMA. STS confirmed the chemisorption of TMA passivated the bandgap states due to dangling bonds. Annealing the TMA-dosed Ge surface decreased the STM observed coverage of TMA sites to 0.4 ML at 250°C, and to 0.15 ML at 450°C. XPS analysis showed that only carbon content was reduced during annealing, while the Al coverage was maintained at 0.15 ML, consistent with the desorption of methyl ($-CH_3$) groups from the TMA adsorbates. Conversely, saturation TMA dosing at RT on the monolayer H_2O pre-dosed Ge(100) surface followed by annealing at 200°C formed a saturation layer of Al-O bonds with an Al coverage a factor of two greater than the TMA only dosed Ge(100). It is proposed that the H_2O pre-dosing enhances the concentration of adsorbed Al and forms thermally stable Al-O bonds along the Ge dimer row, which can serve as a nearly ideal passivation and ALD nucleation layer on Ge(100) surface.

5.2 Introduction

As the complementary metal-oxide-semiconductor (CMOS) devices scale down, a new material with high carrier mobility may be required to substitute for the conventional silicon channel. Germanium is one of the candidates for the new channel material because it has superior electronic properties (higher hole and electron mobility) compared to silicon. However, a high interface trap density between Ge and Ge native oxide has been a challenge in fabricating Ge-channel MOSFET devices even with high-k gate oxide materials, since GeO_x is often incorporated as an interfacial layer [1,2].

To minimize the defect density at the interface of a Ge substrate and a gate dielectric layer, a proper passivation is required for a Ge surface prior to the oxide deposition. Various passivation methods have been investigated including epitaxial growth of Si [3,4], halogenation [5-7], sulfurization [8,9], nitridation [10-12] and oxidation [13-17]. The best results were obtained using a stoichiometric GeO_2 layer typically formed by ozone [15] or high pressure oxidation [16] of a Ge substrate. However, for scaling of equivalent oxide thickness (EOT), the thickness of this passivation layer has to be minimized - ideally to a monolayer (ML), which is very difficult using GeO_2 because of its thermodynamic instability on bulk Ge ($Ge + GeO_2 \rightarrow 2GeO$) [18].

Swaminathan et al. recently reported that the interface quality of a Ge MOS stack was improved when H_2O was pre-pulsed multiple times on a Ge substrate prior to the atomic layer deposition (ALD) of Al_2O_3 [19]. Since the passivation of interfacial defects

was attributed to the formation of Ge-OH bonds, it is likely that one can use H_2O as an alternative oxygen precursor to form an ultrathin passivation layer at relatively low temperature (below 300°C) thereby minimizing suboxide formation [18]. Moreover, in a separate study, H_2O was shown to provide a well-ordered chemisorption monolayer even at RT, without disrupting the surface Ge atoms [20,21]. Therefore, reaction of a Ge surface first with H_2O followed by reaction with a metal precursor (e.g. trimethyl aluminum (TMA)) at RT is expected to provide an ideal monolayer passivation and ALD nucleation on a Ge surface.

To design a process for a scalable passivation layer using H_2O and metal precursors, it is crucial to understand the reactions of both H_2O and a metal precursor with a Ge surface. Since TMA is the most commonly used metal precursor, there have been numerous studies on the ALD reaction of TMA and H_2O on semiconductor surfaces [22]. However, most of studies were focused on Si surfaces, and less is known about the TMA/H_2O reaction with Ge or III-V compound materials [19,23,24]. In addition, the direct reaction of TMA with Si or Ge has not been previously studied since it requires clean (oxygen-free and carbon-free) semiconductor surfaces in a water-free ALD reaction chamber.

In this study, the reaction of TMA on a Ge(100) surface and the effect of H_2O pre-dosing were investigated at an atomic level. The direct reaction of TMA was performed at RT, and the thermal behavior of the reacted surface was studied by annealing at different temperatures. The topographic and electronic structures were analyzed by STM and STS while the relative ratio of surface elements was measured using XPS. To determine the effect of H_2O monolayer functionalization of Ge(100),

TMA dosing was also studied on the H_2O pre-dosed Ge(100) surface, and the surface bonding structures were investigated using STM and XPS.

5.3 Experimental details

A Sb-doped *n*-type Ge wafer (0.005-0.020 Ωcm, Wafer World Inc.) was cut into rectangular pieces (12.5 mm × 4.5 mm) and degreased using ultrasonication with acetone, methanol, and deionized water followed by drying with N_2 gas. Each Ge sample was introduced into an ultrahigh vacuum (UHV) chamber at a base pressure of 2×10^{-10} Torr, and cleaned using several cycles of sputter-anneal process to remove the native oxides. The sputtering of each sample was performed using a 2 keV of Ar^+ ion beam (Model 1403 ion gun, Nonsequitur Technologies) at an incident angle of 45 degrees for 30 minutes. During the sputtering process, the sample temperature was maintained at 500°C using direct heating to avoid the incorporation of trace oxygen on a Ge surface [18]. After each sputtering process, the sample was annealed at 700°C for 20 minutes at a base pressure of the main chamber (2×10^{-10} Torr).

TMA dosing was performed in a separate chamber with a base pressure of 5×10^{-9} Torr. After transferring the sample into the dosing chamber, the TMA vapor (Strem Chemicals, Inc.) was introduced directly onto the sample surface at RT by throttling the valves on the TMA dosing line and the container. The pressure of TMA was measured using an ion gauge, and the exposure of TMA was estimated in Langmuirs (1 Langmuir (L) = 1×10^{-6} Torr · 1 second). The HPLC grade H_2O (Fisher Scientific) dose was also performed at RT in the same dosing chamber, but through a different dosing line, by

controlling the flow of the H_2O vapor using a needle valve. The dosing chamber was baked out at 150°C for several hours before and after replacing the dosing source, in order to avoid the cross-contamination between TMA and H_2O.

After TMA or H_2O dose, the sample was transferred back to the main chamber for a thermal annealing at the base pressure (2×10^{-10} Torr). The ramp rate for the direct heating was controlled at 1°C/sec, while the sample temperature was monitored by a pyrometer.

The *in situ* analysis of the topography of the sample was performed using a STM (LT-STM, Omicron Nanotechnology). The filled-state STM images were obtained using the constant-current mode STM (I_{sp} = 0.2 nA) and applying the sample bias at -1.8 V. The electronic structure of the surface species was measured by STS with a variable-z method using a modulation signal (0.1 V, 650 Hz) from an external lock-in amplifier, while sweeping the sample bias from -1.5 to +1.5 V. The *in situ* monochromatic XPS (XM 1000 MkII / SPHERA, Omicron Nanotechnology) was also used to examine the surface elements and the ratio of their relative intensities with an Al Kα source (1486.7 eV) and a takeoff angle of 30 degrees.

5.4 Results and discussion

A Ge(100) was dosed to near saturation at RT with TMA. Figure 5.1 shows STM and STS results obtained on a Ge(100) surface directly reacted with 10,000 L of TMA. Bright semi-ordered features were observed covering 0.75 ML of the surface in the filled state STM image (green box in Figure 5.1(a)). The vertical rows of the semi-ordered

structures are aligned parallel with the vertical rows of surface Ge dimers, which are observed through pinholes (blue box in Figure 5.1(a)). Examination of the TMA reacted areas reveals that many of the bright sites appear as paired dots with 4~5 Å of spacing. The semi-ordered structure is likely consistent with the dissociative chemisorption of a TMA molecule into a di-methylaluminum (DMA) and a methyl group ($-CH_3$), as shown in the schematic diagram in a green box of Figure 5.1(a). However, detailed modeling studies are required to confirm the proposed structure.

To investigate the electronic structure of the ordered bright sites, STS measurements were performed on bare Ge sites and bright ordered sites (Figure 5.1(b)). It was found that the density of states near 0.7 eV is significantly reduced on the bright sites. The STS is consistent with the dangling bonds on the bare Ge dimers being terminated by the chemisorption of DMA and a methyl group, thereby removing the dangling bond states. Similar phenomena were observed on the H_2O chemisorption sites on a H_2O dosed Ge(100) surface [21]. This again is consistent with the bright ordered sites in Figure 5.1(a) being TMA reaction products which terminate surface dangling bonds and partially passivate the surface. To completely passivate the Ge surface using the TMA chemisorption, the nucleation density of the TMA need to be increased closer to unity.

The thermal behavior of a TMA chemisorption site was examined by annealing a TMA dosed surface in ultrahigh vacuum (below 2×10^{-10} Torr). Filled-state STM images in Figure 5.2 shows a Ge(100) surface dosed with 20,000 L of TMA at RT, and annealed at 250°C and 450°C. A significant decrease in coverage of bright features (from 0.8 ML on as-dosed surface to 0.15 ML on 450°C annealed surface) is observed in the STM

images obtained as a function of the annealing temperature. Schematic diagrams of possible surface structures are also shown on the right side of each STM image. For an as-dosed Ge surface, the dissociative chemisorption and the coordinative bonding of TMA are proposed (case a1 and a2 in Figure 5.2(a)). The chemisorption of TMA (case a1) was already proposed in Figure 5.1(a), found to passivate the surface dangling bonds. The coordinative or dative bond of TMA (case a2) possibly occurs with the electron pair donated from an up-Ge dimer atom [22,25,26]. However, dative bonding is likely to be unstable for long periods in ultrahigh vacuum; therefore, case a1 is the more plausible structure for TMA reaction at RT. Case a1 is also consistent with the known stability of -CH_3 on Ge(100) at RT [27].

On a 250°C annealed surface, the TMA-derived species with a diameter ranging from 4~8 Å cover 0.4 ML of the surface, and three different reaction pathways are considered for these species (Figure 5.2(b)). Recombination of two methyl groups result in monomethylaluminum (MMA, case b1) with C_2H_6 as a byproduct, while recombinative desorption between H and -CH_3 result in surface structures shown in the diagrams of cases b2 and b3 in Figure 5.2(b) with CH_4 as a byproduct. Since C-H bond breaking has a high activation energy and since case b1 and b3 are likely to be approximately 40 kJ/mol more exothermic than b2 based on diatomic bond strengths [28], b1 and b3 are considered to be the most likely structures at 250°C.

On a 450°C annealed surface, bright rows perpendicular to the background Ge dimer rows is observed as in the white box in Figure 5.2 (c). Since similar feature was also observed on the Al deposited Si(100) surface [29], the feature in the white box is assigned as the Al dimer rows. It is likely the residual methyl groups are dissociated

from Al, leaving elemental Al features on the surface. Two different cases of the Al dimer row are shown in the diagram of Figure 5.2 (c); Al dimer on the trough (case c1), and Al dimer on the row (case c2). In both structures, Al is dimerized with another Al atom behind it to the direction into the diagram. Since case c1 has less bond angle strain assuming tetrahedral bonding for Ge, it is considered the more likely structure. Although methyl groups are known to desorb from Ge(100) surfaces at 450^oC [27], a 450^oC annealed surface shows similar structures shown on the 250^oC annealed surface indicating presence of residual DMA or MMA due to insufficient annealing.

To examine the chemical composition of the surface, XPS intensities of surface elements relative to the Ge 3*d* core-level were measured and compared (Figure 5.3 (a)). With a saturation dose of TMA on Ge(100) at RT, the ratio of C:Al was about 2.8:1. By annealing up to 450^oC, the carbon content decreases while Al remains almost same, resulting in the ratio of C:Al as 1.2:1. This is consistent with desorption of methyl or methyl-related byproducts during the thermal annealing, as described in Figure 5.2. The carbon remaining on 450^oC annealed surface is attributed to the residual DMA or MMA species due to the insufficient annealing time (5 minutes).

The Al to Ge ratio being independent of annealing temperature is consistent with the STM coverage of surface species at 450^oC (0.15 ML) being the maximum or nominal coverage of Al for a saturation dose of TMA at RT. It is hypothesized that the steric hindrance of methyl ligands or the chemisorption of methyl groups on Ge surface restrict the nucleation density of Al via the direct reaction of TMA on Ge(100) at RT.

To investigate the effect of H_2O chemisorption on TMA nucleation, XPS measurements were performed on the Ge surface pre-dosed with 1×10^6 L of H_2O,

followed by 60,000 L TMA dose at RT (Figure 5.3(b)). The ratio of O:C:Al was 1.2:2.7:1. Similar to the case of TMA dosed surface, only the C content decreased as the annealing temperature increase. However, the Al to Ge ratio for the TMA+H_2O dosed Ge surface is about a factor of two greater than Al to Ge ratio for the TMA only dosed Ge surface. Furthermore, the ratio of O:Al was invariant with annealing temperature up to 450^oC. This implies that TMA readily bonds on a hydroxyl site at RT, forming a thermally stable Al-O-Ge bond. Since a –CH_3 dissociated from TMA can recombine with a hydrogen atom when TMA bonds on –OH, the steric hindrance of the TMA ligand and the methyl site blocking issues are much reduced compared to the TMA only case.

To verify the bonding structures of the surface, STM measurements were performed on a Ge surface pre-dosed with 7×10^5 L H_2O followed by 35,000 L dosing of TMA at RT (Figure 5.4). Although a poor H_2O dose left a high density of bright dangling bond sites, semi-ordered regions are observed on the surface after annealing at 200^oC, as shown in the white box in the STM image of Figure 5.4. Line profile analysis shows the vertical rows have 8~9 Å of spacing. Considering the symmetry of the bonding structure and the elemental ratio obtained from XPS, a model structure is proposed in the bottom of Figure 5. Since the H_2O dosed Ge surface has one –OH and one –H on each dimer, it is plausible that an Al atom on a Ge dimer will eventually make two bonds; one on a Ge atom directly, and the other on O atom atop of Ge. Further analysis of STM and STS were not available due to the extremely unstable tunneling signal from the surface indicating the formation of ultrathin AlO_x layer.

5.5 Conclusions

Direct reaction of TMA on a Ge(100) surface at RT was investigated at an atomic level, and the thermal behavior of surface species was examined. It is found the TMA chemisorption on clean Ge(100) partially passivates the Ge(100) surface by terminating the surface dangling bonds, but the nucleation density of Al is restricted due to the steric hindrance and substantial adsorption of methyl groups. Poor nucleation density of Al in the direct reaction of TMA on Ge(100) suggests that the oxidant-first ALD initiation should be needed for Ge(100) surface. Monolayer H_2O reaction enhances the nucleation of TMA, maintains a flat surface, and provides a thermally stable Al-O bond which offers a high density initiation layer for other high-k materials. The combination of monolayer H_2O functionalization followed by monolayer TMA doubles the Al nucleation density which may be critical to prevent pinhole formation in the aggressive scaling of gate oxide thickness.

5.6 Acknowledgements

This work is supported by the MSD Focus Center Research Program (2051.001). The authors would like to acknowledge Prof. Wallace group at UT Dallas for their helpful discussions on the XPS experiments.

Chapter 5, in full, is currently being prepared for submission for publication of the material as it may appear in J.S. Lee, T. Kaufman-Osborn, W. Melitz, S. Lee and A.C.

Kummel, 'Atomic Imaging of Nucleation of Trimethylaluminum on Clean and H_2O Functionalized Ge(100) Surfaces', *J. Chem. Phys.* The dissertation author was the primary investigator and author of this material.

.

5.7 Figures

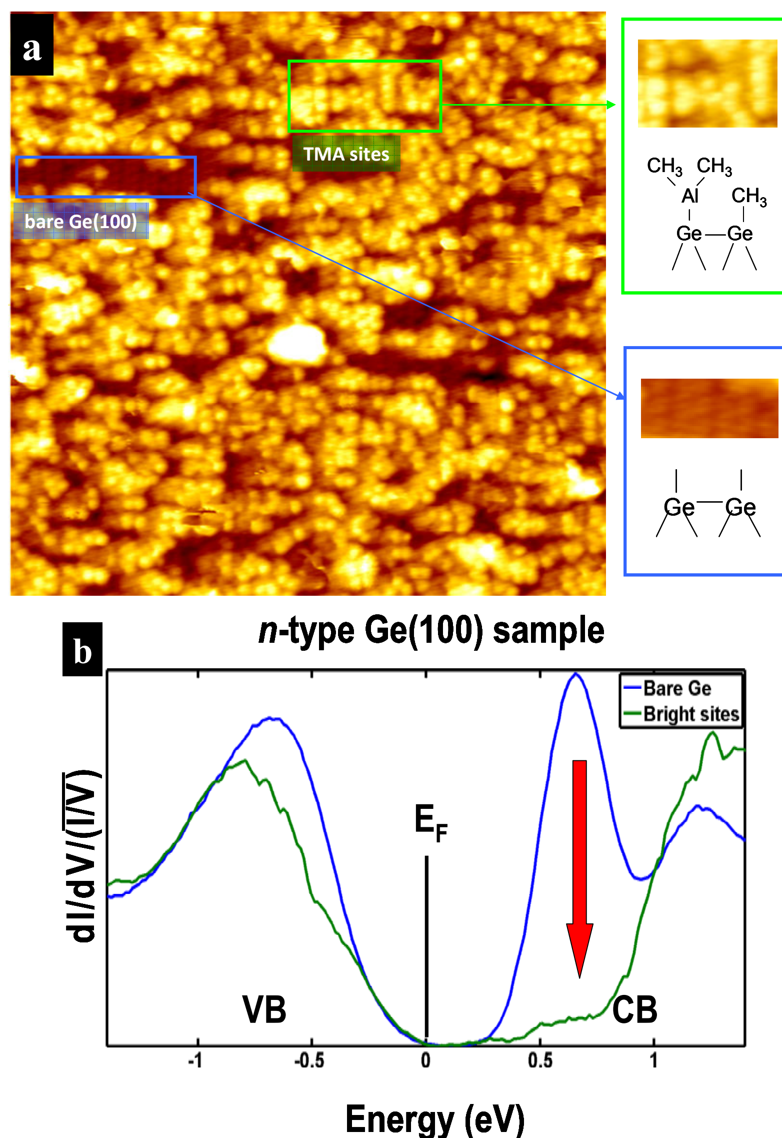

Figure 5.1 STM and STS obtained from a Ge(100) surface dosed with 10,000 L of TMA at RT. (a) Filled state STM image (Vs = -1.8V, It = 0.2 nA, 30 nm × 30 nm) indicates semi-ordered TMA chemisorption sites (green box) and bare Ge(100) sites through pinholes (blue box). Corresponding zoom-in images and schematic diagrams are shown on the right. (b) STS curve measured on bright TMA sites (green) shows a significant reduction of the dangling bond states near 0.7 eV (red arrow) compared to the STS curve measured on bare Ge sites (blue).

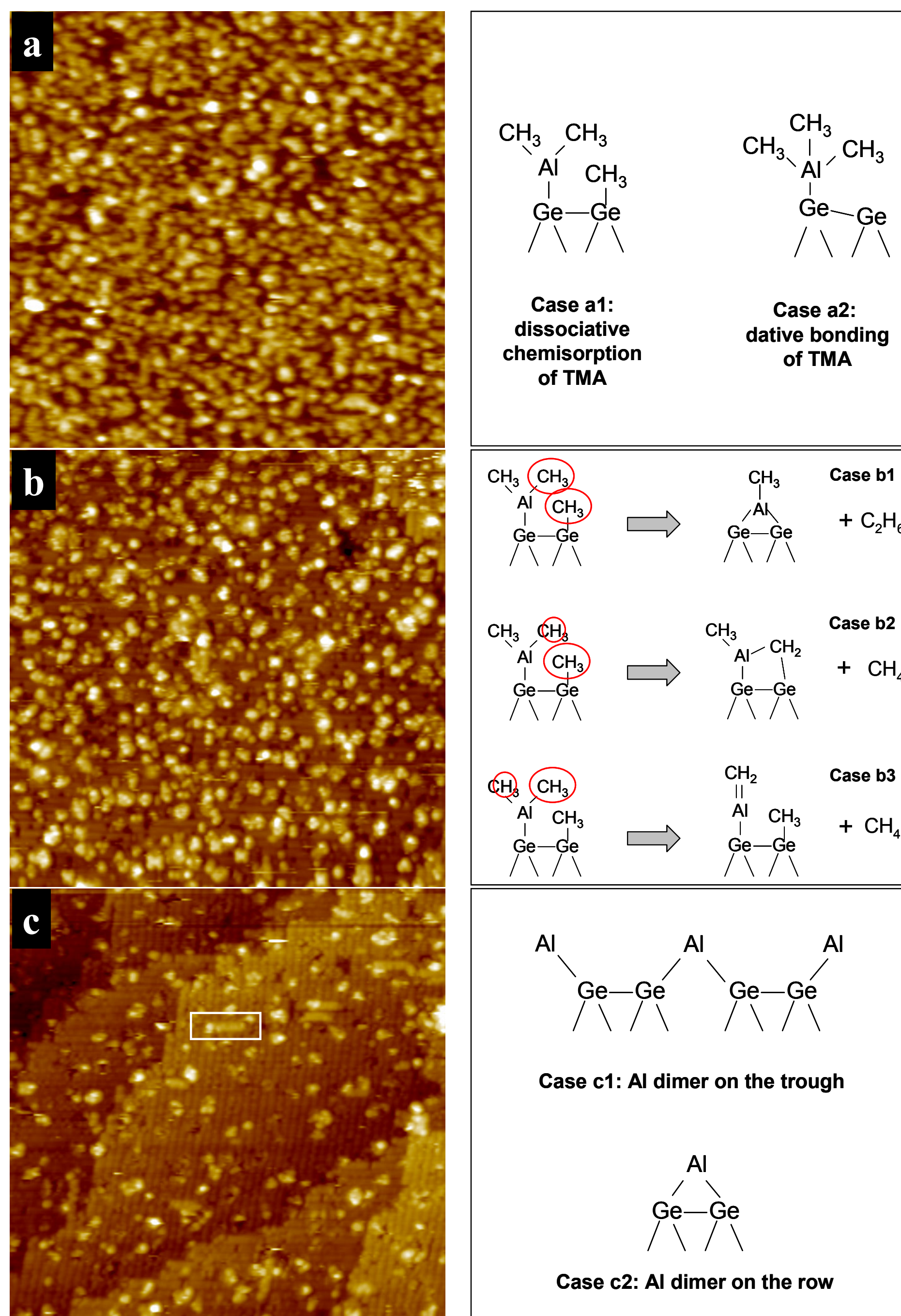

Figure 5.2 STM images (Vs = -1.8V, It = 0.2 nA, 50 nm × 50 nm) and possible structures of a Ge(100) surface dosed with 20,000 L of TMA. (a) As-dosed surface at RT is covered by 0.8 ML of bright TMA sites. (b) The 250°C annealed surface shows TMA-derived species covering 0.4 ML of surface. (c) The 450°C annealed surface has Al rows (white box in the image) perpendicular to the Ge dimer rows. Coverage of surface features is 0.15 ML.

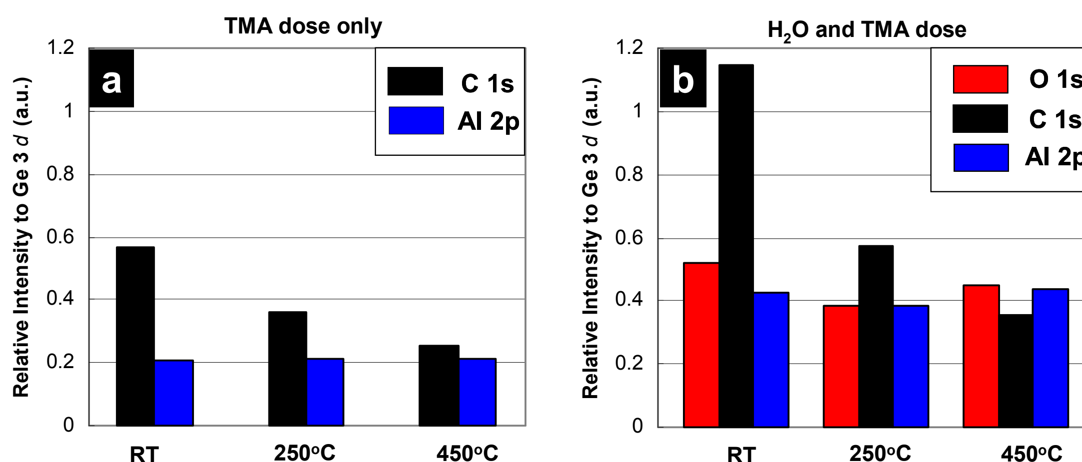

Figure 5.3 Relative XPS intensities of surface elements compared to the Ge3*d* core-level. (a) On a saturation TMA dosed Ge(100) at RT, C:Al ratio is roughly 3:1. By annealing to 450°C, only C content decreases while Al amount remains the same. (b) A saturation dose of H_2O followed by TMA at RT produces 1:3:1 of O:C:Al ratio. By annealing up to 450°C, only C content decreases while O and Al intensities remain the same. Note that the amount of Al increased as a factor of two on the H_2O pre-dosed Ge(100) surface.

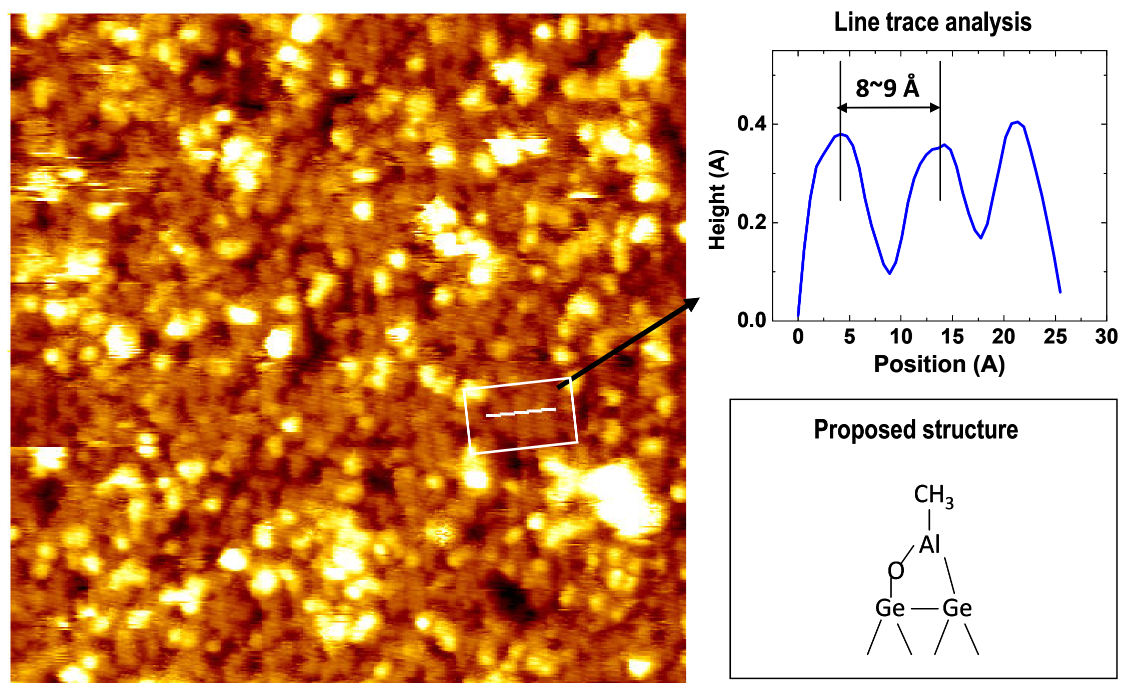

Figure 5.4 Filled state STM image (30 nm × 30 nm) of 7×10^5 L H_2O dosed Ge(100) followed by 35,000 L TMA dosing at RT and annealing at 200°C. An ordered structure is observed (white box). Line profile shows the spacing of vertical rows is ~9Å, and proposed structure is shown on the bottom right.

5.8 References

[1] Y. Kamata, Mater. Today 11 (1-2) (2008) 30.

[2] M. Caymax, M. Houssa, G. Pourtois, F. Bellenger, K. Martens, A. Delabie, S.VanElshocht, Appl. Surf. Sci. 254 (19) (2008) 6094-6099.

[3] B. DeJaeger, et al., Microelectron. Eng. 80 (2005) 26.

[4] N. Taoka, M. Harada, Y. Yamashita, T. Yamamoto, N. Sugiyama, S.-i. Takagi, Appl. Phys. Lett. 92 (11) (2008) 113511.

[5] P. Ardalan, E.R. Pickett, J.S. Harris, Jr., A.F. Marshall, S.F. Bent, Appl. Phys. Lett. 92 (25) (2008) 252902.

[6] S. Sun, Y. Sun, Z. Liu, D.-I. Lee, P. Pianetta, Appl. Phys. Lett. 89 (23) (2006) 231925.

[7] R. Xie, M. Yu, M.Y. Lai, L. Chan, C. Zhu, Appl. Phys. Lett. 92 (16) (2008) 163505.

[8] T. Maeda, S. Takagi, T. Ohnishi, M. Lippmaa, Mat. Sci. Semicon. Proc. 9 (2006) 706.

[9] R. Xie, C. Zhu, IEEE Elec. Dev. Lett. 28 (2007) 976.

[10] H. Kim, P.C. McIntyre, C.-O. Chui, K.C. Saraswat, M.-H. Cho, Appl. Phys. Lett. 85 (14) (2004) 2902.

[11] T. Maeda, T. Yasuda, M. Nishizawa, N. Miyata, Y. Morita, S. Takagi, J. Appl. Phys. 100 (1) (2006) 014101.

[12] T. Sugawara, R. Sreenivasan, P.C. McIntyre, J. Vac. Sci. Technol. B 24 (5) (2006) 2442.

[13] F. Bellenger, M. Houssa, A. Delabie, V. Afanasiev, T. Conard, M. Caymax, M. Meuris, K. DeMeyer, M.M. Heyns, J. of Electrochem. Soc. 155 (2) (2008) G33-G38.

[14] A. Delabie, F. Bellenger, M. Houssa, T. Conard, S. VanElshocht, M. Caymax, M. Heyns, M. Meuris, Appl. Phys. Lett. 91 (8) (2007) 082904.

[15] D. Kuzum, T. Krishnamohan, A.J. Pethe, A.K. Okyay, Y. Oshima, Y. Sun, J.P. McVittie, P.A. Pianetta, P.C. McIntyre, K.C. Saraswat, IEEE Elec. Dev. Lett. 29 (4) (2008) 328.

[16] C.H. Lee, T. Tabata, T. Nishimura, K. Nagashio, K. Kita, A. Toriumi, ECS Trans. 19 (1) (2009) 165-173.

[17] H. Matsubara, T. Sasada, M. Takenaka, S. Takagi, Appl. Phys. Lett. 93 (3) (2008) 032104.

[18] K. Prabhakaran, F. Maeda, Y. Watanabe, T. Ogino, Thin Solid Films 369 (1-2) (2000) 289-292.

[19] S. Swaminathan, Y. Oshima, M.A. Kelly, P.C. McIntyre, Appl. Phys. Lett. 95 (3) (2009) 032907.

[20] J.S. Lee, S.R. Bishop, T. Kaufman-Osborn, E. Chagarov, A.C. Kummel, ECS Trans. 33 (6) (2010) 447-454.

[21] J.S. Lee, T. Kaufman-Osborn, W. Melitz, S. Lee, A. Kummel, Surf. Sci. (submitted).

[22] R. Puurunen, J. Appl. Phys. 97 (12) (2005) 121301.

[23] J.B. Clemens, E.A. Chagarov, M. Holland, R. Droopad, J. Shen, A.C. Kummel, J. Chem. Phys. 133 (15) (2010) 154704.

[24] M. Milojevic, R. Contreras-Guerrero, M. Lopez-Lopez, J. Kim, R.M. Wallace, Appl. Phys. Lett. 95 (21) (2009) 212902.

[25] M.A. Filler, S.F. Bent, Prog. Surf. Sci. 73 (1-3) (2003) 1.

[26] X. Cao, R.J. Hamers, J. Phys. Chem. B 106 (8) (2002) 1840.

[27] P.Y. Chuang, W.L. Lee, T.F. Teng, Y.H. Lai, W.H. Hung, J. Phys. Chem. C 113 (40) (2009) 17447-17454.

[28] CRC Handbook of Chemistry and Physics, Boca Raton, FL, CRC Press/Taylor and Francis, 2010.

[29] J. Nogami, A.A. Baski, C.F. Quate, Phys. Rev. B 44 (3) (1991) 1415.